2018

VALLEY BOTTOM POSITION AND THE OCCURRENCE OF PALEOSOLS AFFECT SOC DYNAMICS

Benedict W. Ferguson
Murray State University

VALLEY BOTTOM POSITION AND THE OCCURRENCE OF PALEOSOLS AFFECT SOIL ORGANIC CARBON DYNAMICS

A Thesis
Presented to
The faculty of the Watershed Studies Institute &
the Department of Earth and Environmental Sciences
Murray State University
Murray, Kentucky

In Partial fulfillment
of the requirement for the degree
of Master of Science

by
Benedict Wade Ferguson
December, 2018

ACKNOWLEDGMENTS

I would like to thank my advisor, Gary Stinchcomb, without his support and guidance this work would not have been possible. I would also like to thank my M.S. committee members; Howard Whiteman, Bassil El Masri, Paul Gagnon, Sung-ho Hong, and William Lukens. Each committee member brought a unique perspective to this work that helped to make this study what it is. I would like to thank Michael Johnson and the staff at the Clarks River National Wildlife Refuge Offices for allowing me access to the refuge and for sharing with me the history of the refuge. I would like to thank Angela Hayden, Gerry Harris and the Watershed Studies Institute for their support. I would like to thank Jennifer Thorn and the faculty and staff of the Department of Earth and Environmental Sciences at Murray State University for all of their support. And finally, I would like to thank the masters and undergraduate students that I worked with during my time here at Murray State University. We spent many hours sharing our experiences and our work with one another, helping to make sure that each of us were doing our best work. This study would not have been possible without funding from the Department of Earth and Environmental Sciences, the Watershed Studies Institute, CISR and a KY NASA EPSCoR grant awarded to Dr. El Masri, Dr. Cetin and Dr Stinchcomb. Isotope analysis was funded using an NSF grant, awarded to Dr. Stinchcomb, and travel funds provided by the Jones College of Science, Engineering and Technology.

ABSTRACT

Soil organic carbon (SOC) storage in depositional zones has been a growing topic of interest in recent years as these areas may be sinks of SOC. However, SOC dynamics greater than 1 m in depth in river valley bottom soils are not well understood. This study examines the soil organic carbon along three alluvial landscape positions in the forested, humid-subtropical setting of the Clarks River in the western Kentucky portion of the Mississippi River basin. These soil and depositional profiles range in age from ~8,000 years ago to modern, 21 cal yr. BP, (BP = AD 2010). The mean surface soil SOC stocks (kg/m^2) decrease from Floodplains (2.62 ± 0.3), Terraces (2.31 ± 0.21) to Bars (1.32 ± 0.24); whereas, the mean stocks of buried layers (buried soils and lithologic discontinuities) decrease from Terraces (4.13 ± 0.24), Bars (3.07 ± 0.54) to Floodplains (2.68 ± 0.24). Total SOC estimates in the buried layers make up over half of the SOC inventory for all landforms. The isotopic composition of SOC ($\delta^{13}C$) at all sites is consistent with C_3 vegetation. The depth profiles show that $\delta^{13}C$ becomes less negative with depth, likely due to a combination of the Suess effect and microbial decomposition. A classification and regression tree analysis shows that soil horizon, pH, landscape position, and magnetic susceptibility are significant predictors of mean SOC content. Notably, the tree shows that alkaline pH (>7.9) is an important predictor in higher mean SOC. These alkaline soil pH values are found in buried calcareous soils with pedogenic carbonate in the Clarks River Terraces, where acidified samples were found to have higher mean SOC. A ^{14}C age from SIC shows that this carbonate may have formed under

drier conditions of the mid-Holocene hypsithermal. This age association suggests that the legacy of buried soils in valley bottoms plays a role in deep SOC storage today. This study showed that buried soils and sediments contain the majority of the SOC in the Clarks River, while landform position and a calcareous paleosol played an important role in the storage of that SOC.

TABLE OF CONTENTS

LIST OF TABLES

LIST OF FIGURES

INTRODUCTION

Soil contains the largest reservoir of active terrestrial carbon (C) (Luo et al., 2017; Leifeld and Kögel-Knabner, 2005; Schimel et al., 1994). This reservoir is relates to climate as C exchanges continuously between the soil, atmosphere and biosphere (Berhe et al., 2007). The dominant processes affecting C in the soil are local redistribution and storage on a landscape scale (Kirkels et al., 2014; Liu et al., 2003; Smith et al., 2001). Thus, when constructing global climate models, understanding long term soil-biosphere-atmosphere interactions and the associated transport and storage of C throughout the soil are key. Despite this importance, uncertainty remains regarding the roles that human-induced soil erosion, topography and deposition play in the biogeochemical cycling of terrestrial C.

1.1. Effects of erosion on soil organic carbon

Topography on Earth's surface and the ensuing erosion partly controls the redistribution of sediments and C (Berhe et al., 2008). The topsoil (A horizons) is rich in soil organic carbon (SOC), where this SOC is transferred and redeposited within the downstream valley bottom (Doetterl et al., 2016; Van Oost et al., 2007; Stallard, 1998). At any individual locality, erosion removes C from soils, whereas deposition of eroded sediments delivers C in colluvial and fluvial systems (Hoffmann et al., 2009).

Stable, mineral-associated SOC can only be relocated in large quantities through soil erosion. Previous work has shown that 70-90 % of eroded topsoil material is

deposited downhill of the source or in adjacent watersheds (Doetterl et al., 2016; Stallard, 1998) and between 53 % and 95 % of eroded SOC remains within the catchment (Kirkels et al., 2014; Van Oost et al., 2007). The decomposition of this SOC after transport varies depending on its fate after deposition (Berhe et al., 2007; Starr et al., 2000). Assuming new vegetation grows on eroded surfaces in the uplands, much of the C that is redeposited downslope is actively replaced, causing the watershed to act as a net C sink (Doetterl et al., 2016; Van Oost et al., 2012; Berhe et al., 2008; Van Oost et al., 2007).

1.2. Effects of deposition on soil organic carbon

Soil burial in river valley bottoms is an important but understudied process that contributes to the delivery and persistence of SOC stocks at depth. The process of soil burial results in C storage at great depths, as buried soils have been observed up to four meters in depth, or greater in some cases (Blazejewski et al., 2009; Chaopricha and Marín-Spiotta, 2014). This process of burial transfers SOC from an active pool to a passive storage pool where rates of SOC turnover are significantly lower after burial (D'elia et al., 2017; Kirkels et al., 2014; Van Oost et al., 2005). Estimates suggest the burial of sediments transfers 10 Gt/yr. and human burial transfers 0.6 – 1.6 Gt/yr. of active SOC to the passive storage pool (Kirkels et al., 2014; Stallard, 1998). Despite recent efforts, these deeper SOC stocks (>30 cm) are typically underestimated (Chaopricha and Marín-Spiotta, 2014; Nadeu et al., 2012).

Large quantities of SOC are stored over long time periods in buried valley-bottom environments with a slow turnover time (Doetterl et al., 2016; VandenBygaart et al., 2015; Wang et al., 2015a, 2015b; Hemelryck et al., 2010; Polyakov and Lal, 2004a,

2004b). With increasing deposition and depth of burial, soil conditions at depth can slow decomposition and reduce C mineralization. Reduced temperature and moisture variability, increased moisture and reduced O_2 levels, combined with physical protection through aggregate formation, all act to stabilize deeper C in depositional settings (D'elia et al., 2017; Kirkels et al., 2014; Berhe et al., 2007, 2005; Van Oost et al., 2005; Liu et al., 2003; McCarty and Ritchie, 2002; Smith et al., 2001; Stallard, 1998).

1.3. Effects of landscape position on SOC dynamics in valley bottoms

Deposition and storage of SOC takes place at various geomorphic positions including colluvial, alluvial, lacustrine, and riverine settings. (Kirkels et al., 2014; Harden et al., 1999; Stallard, 1998). This deposition effects the distribution of C in Floodplains and riparian zones (Chaopricha and Marín-Spiotta, 2014; Kirkels et al., 2014; Blazejewski et al., 2009). A total organic carbon (TOC) study from the Rhine River valley shows that sedimentary facies (changes in texture and sedimentary structures) and associated depositional environments had a significant effect on the soil TOC content (Hoffmann et al., 2009). Net OC accumulation rates in Rhine basin Floodplains exceed hillslopes over the past ~7500 years, and these two landscapes together exceed storage estimates of lakes and reservoirs in Central Europe (Hoffmann et al., 2013), further emphasizing the effects of landform position on SOC dynamics. Despite the findings that alluvial landforms in a river valley could have potentially large effects on storage and cycling of SOC, there are few studies on the effects of alluvial landform position on SOC stocks.

This study examines the effects that alluvial landscape position has on the stock and isotopic composition of SOC in a humid-subtropical setting, along the Clarks River, Kentucky USA. Specifically, we test the hypothesis that C is stored in similar amounts across active alluvial landscape positions and in soils buried within these landforms. To test this hypothesis, we measured C stocks along different alluvial river valley landscape positions associated with different landforms within the Clarks River valley. Other physicochemical properties, such as texture, pH, and magnetic susceptibility, were measured to help determine how landscape position effects C stock variability.

METHODS

2.1. Site Selection

The soil depositional profile sites are selected along the valley bottom of the Clarks River, located in western KY, U.S.A., to examine how different alluvial landforms and the presence of buried soils affected the storage of SOC. Landforms are identified using a combination of LiDAR digital elevation models (DEMs), soils, aerial photography and land cover data (Fig. 1) to develop a basic geomorphic map based on differences in soil series and elevation above the channel.

Three cross-valley transects, referred herein as MZ, TZ and DC, are chosen using the geomorphic map and field reconnaissance, where each transect consisted of three alluvial landscape positions: Bar (MZ_b, TZ_b, DC_b), Floodplain (MZ_f, TZ_f, DC_f) and Terrace (MZ_t, TZ_t, DC_t). An additional Terrace site (CR_t) is selected due to complications in site access at one terrace site towards the end of the field campaign. Transects are selected to replicate factors such as soil series type, proximity to Clarks River, amount and type of vegetation, and elevation.

Each alluvial landform type has surfaces in a defined range of elevations above the river channel, where this range of elevations is herein termed *landform*

relief (Fig. 2). Bars are defined as having low landform relief (<1 m) and located adjacent to or within the main channel. The Bar sites vary in the degree of vegetation and often consist of bedded silt, sand or gravel (Fig. 3). Soils on Bars are mapped as Cascilla Series (Fluventic Dystrudepts), described as well-drained, permeable soils weathering silty alluvium on floodplains (Soil Survey Staff et al., 2001) Floodplains are defined as having moderate landform relief (1-3 m) and located adjacent to the channel. The Floodplain sites have low-sloping surfaces that periodically flooded. Soils associated with Floodplains are also mapped as Cascilla Series. The occurrence of Cascilla Series along both bar and floodplain landforms is likely due to limitations in soil-mapping resolution and the fact that alluvial bars are not an ideal target for soil mapping.

Terraces are defined as having high landform relief (4-5 m) and located further from the main channel. The Terrace sites also have low-sloping surfaces and are flooded only during major flood events. The flood of 2011 suggests the water level was 2 m above terrace floor, based on a road sign marking the water level. Soils along Terrace landforms are mapped as Natalbany Series (Vertic Epiaqualfs), described as poorly drained and slowly permeable soils weathering clayey deposits along floodplains or terraces (Soil Survey Staff et al., 2013b). All alluvial landform sites in this study are situated in a bottomland hardwood, forest ecosystem.

2.2. Soil Sampling and Description

The soil and sediment at each site are sampled at 10-cm intervals until refusal or to a maximum potential depth of ~4 m using a bulk density coring device (Soil Survey Staff, 2009). Refusal at Bar and Floodplain sites is shallower due to the depth of the water table. At depths of approximately 4 m, bulk density core samples at the sites are no longer recoverable due to limitations of the sampling equipment.

Soil horizons are identified and described from auger tailings in the field and refined using laboratory results listed in section *2.3*. Horizons are described using standard descriptive techniques (Schoeneberger, 2012). Buried soils are identified based on the occurrence of distinct genetic horizons that experienced pedogenesis and subsequently buried by new sediment. Lithologic discontinuities (LDs) are also identified separately from buried soils. The identification of LDs follows the definition in Ahr et al. (2016) as abrupt changes in geologic layering not associated with pedogenesis. These changes are often the result of differing parent materials brought on by changes in depositional environment. An LD may also be associated with the occurrence of a buried soil. This study combines the observations of both buried soils and LDs, and they are together referred to herein as *buried layers*. The modern, or surface, soils are then separated from buried layers based on the depth to the first buried soil or LD and are discussed separately from the buried layers.

Radiocarbon ages are used to estimate landform age. Charcoal and carbonate samples are collected at all sites for ^{14}C analysis. Samples are analyzed using a NEC Pelletron 500 kV accelerator mass spectrometer at a commercial lab (Direct AMS). Modern (post-bomb) radiocarbon ages are modeled using CALIBomb (Stuiver and Reimer, 1993) and pre-bomb ages are calibrated using CALIB 7.1 (Reimer et al., 2013).

2.3. Laboratory measurements

2.3.1. Soil and sediment characterization

The physical, chemical and mineralogical characteristics of soil and sediment are measured to determine what factors effected the SOC content among the three alluvial landforms. These characteristics are then analyzed with depth in both surface soil and buried layers for the <2mm size fraction. Soil texture and bulk density are important determinants of water retention and C storage potential of a soil (Bullinger-Weber et al., 2014; Jobbágy and Jackson, 2000). Texture is determined using a modified micro-pipette method (Soil Survey Staff, 2014a). The results are reported in concentrations of clay, silt and sand. Oven-dry bulk density (ρ_d) is measured using the core method (Soil Survey Staff, 2009).

While texture is a proxy for SOM retention, soil pH is more related to SOM stabilization and protection (Rasmussen et al., 2018). Soil pH is measured using 1:1 soil:H_2O and 1:2 soil:$CaCl_2$ (Soil Survey Staff, 2014a; Miller and

Kissel, 2010). Electrical conductivity (EC) is measured by direct saturated paste (Soil Survey Staff, 2014b). The magnetic susceptibility of soil is a measure of the concentration and grain size of magnetic minerals in a sample and is a proxy for soil development, notably redox(Maxbauer et al., 2017; Grimley et al., 2004; Fine et al., 1995). Room-temperature mass-dependent susceptibility (X) is measured at two frequencies on dry soil and sediment using a Bartington MS2B magnetic susceptibility meter. Low-frequency (X_{lf}, 450 Hz) and high-frequency (X_{hf}, 4.5 kHz) susceptibilities are used to calculate frequency-dependent susceptibility (X_{fd}), which is a measure of the concentration of superparamagnetic (SP) particles in the soil (Dearing, 1994). The X_{fd} is calculated as:

$$X_{fd} = \frac{X_{lf} - X_{hf}}{X_{lf}} * 100 \qquad \text{Eq. 1.}$$

2.3.2. C measurements and calculations

The SOC is measured on a subset of acidified samples (n=64) using dry combustion on a CHNS-O Costech Elemental Analyzer. The SOM is measured on all samples using the loss on ignition (LOI) method (Soil Survey Staff, 1996). Oven-dried samples are analyzed for total combustion of organic matter at 650° C for 6 hours.

Adapting the methods of Andrews et al.(2011), the more extensive LOI data set and the SOC data set, and clay content are used to derive a correction factor to convert SOM to SOC. The correction factor is developed using a

pedotransfer function similar to that of Hoogsteen et al. (2015) because LOI can result in the dihydroxylation of clay, i.e., structural water loss, and the overestimation of SOM/SOC content. A regression model is used to model SOC (wt. %) using LOI and clay (wt. %) as predictors (Appendix 13).

SOC stocks are calculated for each horizon using the following equation:

$$\boldsymbol{SOC_{stock}} = \frac{\boldsymbol{SOC}}{\mathbf{100}} \times \boldsymbol{\rho_d} \times \boldsymbol{z} \ , \qquad \text{Eq. 2}$$

where SOC_{stock} is in kg/m^2, SOC is in wt %, ρ_d is in kg/m^3 and z is the soil horizon thickness in meters. If there is more than one sample per horizon, then the mean SOC for that horizon is reported. The SOC stocks discussed here are minimum estimates for both the surface and buried soils. While the surface soils were sampled in their entirety, the depth of the surface soils and the distinction between surface and buried is complex. During soil sampling and description, overprinting from overlying horizons was noted, and as a result, underlying buried soil horizons likely experienced some translocation of C into these buried layers. The determination of the lower boundaries of the surface soils is based on the first occurrence of buried horizons. In regards to the buried layers, no sites are sampled to bedrock and so buried layers likely have more, deeper SOC.

The isotopic composition of soil organic carbon ($\delta^{13}C_{soc}$) is measured on a subset of samples (n=64) to provide insight into the source of the SOC and effects of decomposition. Samples are ground in a mortar and pestle and treated with 1N

HCl to remove any inorganic carbon (calcite). The samples are then triple-rinsed in deionized water and then the SOC is combusted in a CHNS-O Costech elemental analyzer. The resulting CO_2 is analyzed by continuous flow using a Finnigan Thermo-Electron gas-source mass spectrometer (standard error, ± 0.01‰). The values are reported here in ‰, with reference to the Pee Dee Belemnite standard (VPDB), using the equation:

$$\delta^{13}C_{soc}(‰) = \left\{ \left[\left(\frac{^{13}C_{sample}}{^{12}C_{sample}} \right) \Big/ \left(\frac{^{13}C_{VPDB}}{^{12}C_{VPDB}} \right) \right] - 1 \right\} * 1000 \qquad \text{Eq. 3.}$$

2.3.3. Statistical Analysis

The chemical, physical, and mineralogical properties along with the SOC content of the alluvial landforms are compared by surface and buried soils by alluvial landform using Analysis of Variance (ANOVA) with a *post-hoc* Tukey's Honest Significant Difference test (Tukey HSD) (R Core Team, 2017). Rejection of the null hypotheses (means are the same for all groups) using ANOVA and Tukey HSD is set to the 95 % confidence level ($\alpha = 0.05$). The associations between alluvial landscape position, SOC and other soil properties are explored further using a classification and regression tree which uses a recursive partitioning procedure (Prasad et al., 2006).

Classification and regression trees (CART) are developed in R using the rpart package (Therneau et al., 2018). The regression tree is created to rank the soil properties and landform position in importance of predicting SOC by determining the best predictor with respect to the response variable and dividing the observations (Prasad et al., 2006; Scull et al., 2005). This division reduces the variance in the response variable and is repeated until the observations are exhausted. Predictors used to estimate SOC are landform position, horizon designations, layer descriptions (surface v buried), sample thickness, ρ_d, pH (1:1 H_2O), EC, X_{lf}, and X_{fd}. Because an SOC correction factor is applied using LOI and clay content (see *2.3.2.*), LOI and grain size (sand, silt, clay) are excluded from CART analysis to prevent autocorrelation between SOC and the predictors.

Prediction error is estimated by randomly dividing the total dataset (n=185) into a 70/30 split: 70 % training sample set and 30 % testing sample set. The regression tree is built using the training set and then 'pruned' by selecting the number of splits produced by the regression tree associated with a minimized cross-validated error estimate (Prasad et al., 2006; Scull et al., 2005). The testing set is then passed through the pruned tree to calculate root mean square prediction error (RMSPE) as a measure of the accuracy of the model in predicting mean SOC:

$$\sqrt{\frac{\sum_i^n (\hat{y}_i - y_i)^2}{n}} \quad \text{Eq. 4}$$

where $\hat{y}$ is the SOC value predicted by the model, y is the known SOC value, i is a given observation, and n is the number of observations in the testing set.

RESULTS

3.1. Geomorphology and geochronology

The Bar, Floodplain and Terrace landforms along the Clarks River vary in elevation, age and soil properties (Fig. 6, Table 1). Surface elevation and landform relief increase from Bars to Floodplains and then to Terraces. Increasing elevation and relief coincide with increasing thickness of the underlying soil and sediment assemblage. The Bar sites: MZ_b, TZ_b and DC_b, have surface elevations between 98 and 99 m above sea level (asl). The sample depths range from 0.3 to 1.5 m below the surface, where the water table or refusal was reached (Fig. 2). The Floodplain sites: MZ_f, TZ_f and DC_f, have surface elevations ranging from 98 to 100 m asl. The sample depths range from 2 to 2.8 m below the surface, where coring reached refusal. The Terrace sites: MZ_t, TZ_t, DC_t and CR_t, have a narrow range of surface elevations at ~103 m asl. The sample depths for Terrace sites, MZ_t and TZ_t, are 4 m below the surface, where ground water or refusal made further soil/sediment extraction difficult. The sample depths of the DC_t and CR_t sites are 1.5 m and 2 m below the surface, respectively, due to logistical constraints.

Median radiocarbon ages from the three alluvial landforms vary in age from 8,036 to 21 cal. yr. BP, where cal. yr. BP is calendar years before present; present = AD 2010 (Table 1). Woody debris (Fig. 4) from MZ_b at 1.3 m in depth is 21 yr. BP, modeled using bomb-pulse dating (Stuiver and Reimer, 1993).

Charcoal from 2.5 m below the surface along a Floodplain (MZ_f) yields a modeled age of 666 cal. yr. BP. Pedogenic carbonate from 3 m below the surface (100 m asl) along a Terrace (MZ_t) yields the oldest modeled age of 8,036 cal. yr. BP. A charcoal sample from 0.6 m below the surface in a Terrace (TZ_t) yields a modeled age of 447 cal. yr. BP. All calibrated ages are lower in elevation and younger than a late Pleistocene near-shore strandline deposit (108 m asl) that marks the water-surface elevation of pro-glacial lake Paducah, which occupied the Clarks River valley 21,080 ± 400 radiocarbon yr. BP (Olive, 1966). This radiocarbon age has a modeled median age of 25,385 cal. yr. BP (Reimer et al., 2013).

3.2. Physical, chemical and mineral characterization

3.2.1. Bars

Surface soil and sediment profiles on Bars are shallow, <0.60 m deep, and range from no soil development on the TZ_b to gleyed topsoil (Ag) and subsoil (Bg) development at the MZ_b and DC_b sites (Fig. 5). The MZ_b and DC_b soils coarsen upwards and have a silty clay loam texture. The TZ_b sediment has sandy clay loam texture. The mean (± standard error of the mean) ρ_d for Bar soil and sediment is 0.94 ± 0.06 g/cm^3. Bar soil pH values are strongly acidic, 5.5 ± 0.1, whereas the sediment pH values at TZ_b were moderately acidic, 5.9 ± 0.2. All Bar soil and sediment are non-saline, with EC values <0.5 mS/cm. The magnetic properties of Bar soil and sediment show little variability with depth and have a mean X_{lf} and X_{fd} of 1.97 ± 0.17 x 10^{-7} kg/m^3 and 8.1 ± 0.34 %, respectively (Fig. 6).

Buried layers in the Bars include two buried soils in the MZ_b and geologic layering in the DC_b site (Fig. 5). The TZ_b does not contain any buried layers. The uppermost buried soil in the MZ_b is 0.98 m thick and likely overprints the underlying buried soil. These buried soils are gleyed like the overlying surface soil. The 2Cg2 horizon in the DC_b is 0.20 m thick, underlying a lithologic discontinuity (LD) at 0.34 m, and is identified by an increase in color value and chroma, and grain size. Like the Bar surface soil, the mean texture of the buried layers is silty clay loam and coarsens upward. The mean ρ_d of the buried layers are 1.08 ± 0.04 g/cm^3, within error of the mean surface soil bulk density. The pH and EC of the buried layers is nearly identical to those of the surface soil, 5.4 ± 0.1 and 0.20 ± 0.04 mS/cm. Like the magnetic properties of the surface soil, buried layers show little variability. However, the buried layers are enhanced, with a mean X_{lf} and X_{fd} of 2.94 ± 0.14 x 10^{-7} kg/m^3 and 9.2 ± 0.26 %, respectively.

3.2.2. Floodplains

Surface soil on Floodplains are shallow (< 0.55 m deep) and have weak subsoil development (Bw) at all sites (Fig. 5). Floodplain surface soils are silty clay loam, whereas the DC_f soil has a silty clay texture and all Floodplain soil coarsens upward. The mean dry ρ_d for the Floodplain soil and sediment are 1.05 ± 0.03 g/cm^3. Floodplain soil pH values are extremely acidic, 4.4 ± 0.1. All Floodplain soil and sediment are non-saline, with EC values <0.5 mS/cm. The magnetic properties of the Floodplain soil and sediment show an increase with depth and have a mean X_{lf} and X_{fd} of 3.33 ± 0.26x10^{-7} kg/m^3 and 9.1 ± 0.26 %, respectively.

Buried layers in the Floodplains include two buried soils in the MZ_f, 1.0 and 1.24 m thick, two buried soils in the TZ_f, 0.98 cm and 0.63 m thick, and three sediment layers each with one buried soil in the DC_f, 0.98, 1.02, and 0.30 m thick (Fig. 5). These buried soils are weakly developed and gleyed like the overlying surface soil. The mean texture of the buried layers is silty clay loam and fine upwards. The mean ρ_d of the buried layers is 1.24 ± 0.01 g/cm^3. The pH of the buried layers is nearly identical to those of the surface soil, 4.2 ± 0.11. The mean EC of the buried layers are non-saline, decreasing with depth to a mean of 0.14 ± 0.01 mS/cm. Unlike the surface soil, buried layers show a depletion of magnetic minerals with depth, with a mean X_{lf} and X_{fd} of 2.19 ± 0.20 x 10^{-7} kg/m^3 and 7.1 ± 0.45 %, respectively.

3.2.3. Terraces

Surface soils forming on Terraces are shallow, <0.70 m depth, and are well developed (O, A, AB, EB, and Btg horizons) (Fig. 5). Terrace surface soil have silty clay texture and coarsen upward. The mean ρ_d for the Terrace soil and sediment was 1.20 ± 0.03 g/cm^3. Terrace surface soil pH is strongly acidic, 4.0 ± 0.10 and non-saline, with EC values <0.5 mS/cm. The surface soil magnetic properties show little variability with depth and are lower than the Bar and Floodplain surface soil and sediment. The mean Terrace X_{lf} and X_{fd} is 1.26 ± 0.09 x 10^{-7} kg/m^3 and 4.0 ± 0.3 %, respectively.

Buried layers at Terrace sites include two buried soils in the MZ_t that are 1.09 m and 0.97 m thick and a geologic layer at the base of the profile that is 0.09 m thick (Fig. 5). The TZ_t has four buried soils that are 1.01, 1.16, 0.46, and 0.82 m thick. The

lowermost three of these buried soils occur within a LD. The third buried soil is a buried ACk horizon between two Ck horizons. The DC_t site contains one identified buried layer 0.61 m thick but likely contained more, due to incomplete sampling. CR_t contains one buried soil 0.84 m thick underlying a LD at 1.0 m below the surface. The mean texture of the buried layers is silty clay and they coarsen upward. The mean ρ_d of the buried layers is 1.33 ± 0.01 g/cm^3, slightly denser than Terrace surface soil. The mean pH of the buried layers, 6.7 ± 0.2, is less acidic than the Terrace surface soil and becomes alkaline with increasing depth and the presence of soil carbonate. Terrace buried layers are non-saline, with a mean EC of 0.90 ± 0.05 mS/cm, but higher than the Terrace surface soil. The buried layers have a mean X_{lf} and X_{fd} of 1.54 ± 0.07 x 10^{-7} kg/m^3 and 1.6 ± 0.17 %, respectively. The magnetic properties of the buried layers show an enhancement of X_{lf} and X_{fd} associated with two buried soils at similar depths (0.70 and 2.75 m below surface) in vertical succession at both MZ_t and TZ_t.

3.3. Soil organic matter characterization

3.3.1. Bars

Bar vegetation varies from forest with grass understory (MZ_b) to sparse vegetation on gravel Bars (TZ_b and DC_b) (Fig.3). The surface soil and sediment SOM vary as well. The MZ_b site has the highest mean SOM, 6.11 ± 0.81 %, while the TZ_b and DC_b sites have similar mean surface SOM, 3.83 ± 0.76 % and 3.87 ± 0.15 %, respectively. The surface SOM decrease with depth in all but the DC_b site. The overall mean Bar SOM content is 4.79 ± 0.52 %. With the exception of TZ_b, where SOC content

initially increased with depth, surface SOC content decreases with depth. Mean surface SOC stocks for the MZ_b and DC_b sites are within error of each mean stock, 1.48 ± 0.37 and 1.90 ± 54 kg/m^2 respectively. While SOC content decreases, SOC stocks increase in all sites with depth with an overall mean surface stock of 1.31 ± 0.24 kg/m^2 (Fig.7).

Buried layers in the Bars have a very similar SOM content compared with the surface soils. Buried layers have a mean value of 4.65 ± 0.19 % at the MZ_b site and a mean value of 4.0 ± 0.14 % at the DC_b site and an overall mean of 4.53 ± 0.18 %. With the exception of TZ_b, SOC content in the buried layers ares very similar to that of the surface soil with DC_b increasing with depth. The MZ_b site has the highest buried SOC stock of the Bar sites with a mean value of 3.49 ± 0.57 kg/m^2. The buried layers in the Bars have an overall mean stock of 3.07 ± 0.54 kg/m^2 (Fig.7).

3.3.2. Floodplains

Floodplain vegetation is forest with a dense understory. Surface soil SOM content decreases with depth and varied little across sites, with a mean content of 4.47 ± 0.23 %. Like SOM content, SOC content in the surface soil decreased with depth and varied little with depth as it decreased. Surface stocks did increase with depth having an overall mean value of 2.62 ± 0.3 kg/m^2 (Fig.7).

Mean SOM contents of the buried soils in the Floodplain sites vary little across sites and decrease with depth. The overall mean value was approximately half that of the surface soils: 2.68 ± 0.09 %. At the MZ_f site the SOC content decreases and then increases slightly with the occurrence of two buried layers (Fig.4). In contrast to the

surface soils and sediments, SOC stocks decrease with depth in the buried layers, with an overall mean stock of 2.68 ± 0.24 kg/m^2 (Fig.7).

3.3.3. Terraces

Terrace site vegetation consists of post oak hardwood forests with very little understory vegetation. The surface soil SOM of the Terraces is within error of the mean across all sites; with the highest mean at the MZ_t site (5.38 ± 0.58 %) and the lowest mean at the DC_t site (4.71 ± 0.40 %). Surface soils have a mean SOM content of 4.91 ± 0.23 % that decreases with depth in all Terrace sites. SOC content decreases with depth in the surface soils. Terrace sites have an overall mean surface stock of 2.31 ± 0.21 kg/m^2 (Fig.7). However, surface SOC stocks increase with depth, the highest being at the MZ_t site (3.35 ± 0.50 kg/m^2) and the lowest at the TZ_t site (1.74 ± 0.22 kg/m^2).

Terrace SOM content increases in buried layers 3 m deep in the MZ_t and the TZ_t sites. SOM content of buried layers is statistically similar to surface SOM. Unlike the surface SOM, the highest and lowest SOM of the buried layers were in the TZ_t and the CR_t sites; 4.97 ± 0.24 % and 4.31 ± 0.13 %, respectively. The mean SOM content of the buried layers is 4.69 ± 0.13 %. SOC content in the buried layers decreases with depth until a depth of approximately 2.75 m where the SOC content increases, reaching SOC concentrations similar to that of the surface soils. Buried stocks have an overall mean value of 4.13 ± 0.24 kg/m^2 (Fig.7). At all sites, the buried stocks increase with depth but vary with horizon thickness.

3.3.4. Isotope geochemistry of SOC and SIC

The $\delta^{13}C_{soc}$ of all surface and buried layers from all landforms ranges from −23 to −29‰, which is consistent with aboveground vegetation using the C_3 photosynthetic pathway (Diefendorf et al., 2010; Kohn, 2010). The $\delta^{13}C_{sic}$ from the 8,036-year-old pedogenic carbonate is −10.8‰. This is consistent with the $\delta^{13}C_{soc}$ values when using a 14-17‰ fractionation factor between plant-derived soil CO_2 and pedogenic carbonate (Quade et al., 1989; Cerling, 1984). This shows that the aboveground vegetation 8,000 yrs ago were also using the C_3 photosynthetic pathway

The SOC content and C/N decrease and $\delta^{13}C_{soc}$ values become less negative (enriched in ^{13}C) with increasing depth on all landforms (Fig. 8). This trend is consistent with calculations for mean $\delta^{13}C_{soc}$ of surface and buried layers for bars (surface = −26.4 ± 0.2‰; buried = −24.9 ± 0.02‰), floodplains (surface = −27.2 ± 0.4‰; buried = −25.2 ± 0.3‰) and terraces (surface = −26.2 ± 0.3‰; buried = −25.5 ± 0.2‰). The difference between surface and buried mean $\delta^{13}C_{soc}$ range from 1.5‰ in the bars, 2‰ in the floodplains and 0.7‰ in the terraces. The SOC turnover rates were also examined for each landform using β, the slope of the line of $\delta^{13}C_{soc}$ to log[SOC] (Acton et al., 2013). Less negative β indicate longer turnover times compared to slopes with a more negative β. The Terrace sites have the least negative slope (β = -1.50 ± 0.38) with slower turnover rates compared to the Bar (β = -2.23 ± 0.77) or Floodplain sites (β = -2.43 ± 0.53). While is less negative β in the Terraces, all three of the slopes are within error of the means. The $\delta^{13}C_{soc}$ values, plotted against SOC and C/N, show no discernible trends or clustering by landform, soil horizon or parent material (C horizons) (Fig.8).

3.4. Statistical Test and Classification and Regression Tree

The surface soil SOC are similar when compared by landscape position (F = 1.545, p = 0.162) (Fig. 9A). However, buried layer SOC did differ by landscape position (F = 9.784, p = 1.54 x 10^{-10}) (Fig. 9B) Post-hoc tests show that buried layer SOC differs by terrace vs. bar (p = 0.038) and floodplain vs. bar/terrace also differ (p <0.0001).

The pruned classification and regression tree results show that cross-validated error was minimized using 5 splits, with a prediction error of 0.24 wt. % (Fig. 10). The tree results show that soil horizon (= B, C) is the first predictor, with a mean SOC of 1.6 ± 0.21 wt. %. The pH (<7.9) is the second predictor, with a mean SOC of 1.2 ± 0.09 wt. %. Landscape position (Floodplain = yes/no) is the third predictor, with a mean SOC of 0.65 ± 0.02 wt. % and magnetic susceptibility (X_{lf} <2.37x10^{-7} kg/m^3) is fourth and last predictor, where observations with a X_{lf} >2.37x10^{-7} kg/m^3 have a mean SOC of 0.59 ± 0.03 wt. % and observations with a X_{lf} <2.37x10^{-7} kg/m^3 have a mean SOC of 0.25 ± 0.02 wt. %. Predictors not useful for estimating SOC are landscape position, layer descriptions (surface v buried), sample thickness, ρ_d, EC, and X_{fd}.

DISCUSSION

Radiocarbon results shows the youngest observed age is from a low-relief bar and the oldest observed age from a high-relief terrace. This is consistent with the common knowledge that older alluvial landforms (Terraces) are found at higher elevations than younger alluvial landforms (Bars), as well as first-principles of relief and age of geomorphic surfaces and underlying landforms (Ritter et al., 2002). This increasing age of landform with increasing relief is further supported by the appearance of clay coatings, more prominent soil structure and lower surface soil pH in the Terraces. These are all indicators of greater, more prolonged, soil development relative to the Bars and Floodplains. An exception to this is the fact that alkaline soils occur in the buried layers of the Terraces due to the occurrence of carbonate rhizoliths (Fig. 4).

4.1. Effects of alluvial landscape position on soil carbon

Total and mean SOM and SOC concentrations and stocks differ significantly between the Bar, Floodplain and Terrace landforms (Tables 2-5). Total SOC inventories increase with increasing observed landform thickness: Terrace > Floodplain >Bar. Although the thickness trend is biased by the sampling depths and refusal, when examining the proportion of total surface soil SOC to the minimum buried layer SOC, buried SOC was 68 % of the total SOC in the Bars, 79 % of the total SOC in the Floodplains, and 83 % of the total SOC in the Terraces (Fig. 8A). At all three landscape

positions, the minimum estimate of total SOC in buried layers (soil and LDs) makes up over half of the total SOC inventory for that landform. Terraces have the greatest proportion of buried SOC and are also the oldest valley bottom landforms. This age may play a role in soil development and SOC storage as older, more developed, soils contain older C or C that is cycling more slowly (Lawrence et al., 2015).

Bars and Terraces have higher mean SOC stocks in their buried layers than Floodplains. By contrast, Floodplains have the highest mean surface stock. Two of the three Bar sites (TZ_b and DC_b) are composed mostly of river-derived gravel and sediment or sediment from bank erosion that has little to no soil development. Bar sites also contain fragments of woody debris (Fig. 4), indicating rapid burial and storage of OC contributing to their high SOC stocks in otherwise OC-poor sediments. Due to the young age of the Bars, the SOC may be young and labile C that has yet to decompose.

The MZ_b site, having greater soil development and a much thicker profile than the other Bar sites, skews the mean SOC stocks for the Bars because it has a much greater SOC content. Intriguingly, a radiocarbon age (Table 1) shows that this MZ_b site has a median age of 21 years BP, where this sample was collected from 1.3 m below the surface. This shows that even though alluvial Bars make up far less area than Floodplains and Terraces, rapid deposition promotes SOC burial to the point that the mean SOC per unit area exceeds the more spatially extensive Floodplain.

Bar sites likely vary in SOC density due to differences in texture, bulk density, and SOC inputs. This variability is largely a function of hydrodynamic effects due to proximity to the Clarks River channel, which affect observed SOC storage. For example, differences in flow velocity along inside and outside meander bends, woody debris

obstructions, large bank erosion slumps and catastrophic stripping of flood chute material (Nanson, 1986) may all contribute to the textural variations in the Bar soil and sediment. This textural variation would affect SOC concentrations. Woody debris (<2mm) (Fig. 4) is also present; it may take longer to decompose due to anaerobic conditions resulting from higher moisture levels (Sutfin et al., 2016; Berhe et al., 2007). The presence of woody debris may also increase the SOC stocks in the < 2 mm fraction as there may be debris 2 mm or smaller in size. However, this woody debris is not noted at all Bar sites and thus represents a heterogenous source of SOC.

Floodplain sites have high surface SOC content that decreases with depth into the associated buried layers. This low SOC content in the buried layers may be due to lack of soil development. The Floodplain sites all have dense understories that may produce high inputs of C at the surface from shallow roots (Rumpel and Kögel-Knabner, 2011; Jobbágy and Jackson, 2000). The top 1.5 meters of the Floodplains also have a higher relative magnetic susceptibility than Bars and Terraces, indicating a better drained soil profile where oxidation would minimize SOC retention (Grimley et al., 2004). The subsequent decrease in magnetic susceptibility and the occurrence of redoximorphic features below 1.5 m suggests a more poorly-drained portion of the profile. This depth to a more poorly-drained portion of the profile is possibly related to water table height. The decrease in SOM and SOC contents lessens with SOM contents remaining at ~2 wt % and SOC content remaining at ~0.25 wt % until the end of the profiles.

Although Floodplains Clarks River valley may have greater inputs of SOC into the surface soil, the weakly developed and poorly structured buried layers may not have the physical or chemical properties needed to retain the high inputs of SOC. This lack of

characteristics needed to retain SOC facilitates SOC oxidation at depth in the buried layers (Doetterl et al., 2016). Only in deeper buried layers did poor drainage appear to slow the loss of SOC, promoting SOC retention.

The Terraces experience infrequent flooding and prolonged landscape stability due to their higher landform relief and distance from the channel. This greater stability allows for greater soil development (Vervoort et al., 1999). The Bt horizons in the Terrace sites suggest clay translocation likely facilitated soil aggregate formation in the subsoil and in buried layers (Bullinger-Weber et al., 2014; Leifeld and Kögel-Knabner, 2005). This increased aggregate formation promotes increased soil structure in the Terraces (Post et al., 2004; Rasmussen et al., 2005). The relatively lower magnetic susceptibility values in the Terrace in the first 2 m of the profiles compared to Bars and Floodplains at similar depths suggests poor drainage (Grimley et al., 2004). This low X_{lf} was consistent with the presence of redoximorphic features in Terrace field descriptions and the mapped soil series for these sites - Natalbany series: fine, smectitic, thermic Vertic Epiaqualfs (Soil Survey Staff et al., 2013). It is likely that the clay and silt-rich LDs at depth in the Terrace soils act as restrictive boundaries between layers, creating prolonged perched water conditions. Increased soil moisture due to poor drainage has been linked to increased SOC accumulation (Grimley et al., 2004).

The deep Terrace SOC is further stabilized by these aggregates, and in combination with available Fe and Al in the acidic layers as well as the exchangeable Ca in the deeper calcareous layers, help bind SOM and promote C stabilization (Rasmussen et al., 2018). The calcareous layers are characterized by soil carbonate rhizoliths (Fig. 4) that were formed approximately 8,000 years ago under soil-forming conditions that

differed from today (Cerling, 1984; Driese et al., 2008). The presence of soil carbonate is not an uncommon occurrence as researchers in the lower Mississippi River basin to the west and middle Tennessee River basin to the east document the occurrence of soil carbonates in buried soils during the middle and late Holocene (Cox et al., 2004; Driese et al., 2008). These buried soil carbonates and the surrounding calcareous sediment in the Clarks River valley promote alkaline conditions which facilitates deep SOC storage. Consequently, there is a legacy effect from past Holocene climates and soil-forming environments that play a direct role in the storage of SOC today.

4.2. Classification and Regression Tree (CART) Analysis of SOC

The pruned regression tree analysis shows that landform type predicts SOC but is less influential than soil horizon and pH (Fig. 10). The selection of A horizons in the model yields the highest predicted mean SOC wt. % (1.6 wt %), consistent with the Clarks River valley SOC. The second predictor is pH and is indirectly linked with alluvial landform position and buried soil. The soil pH $\geq$ 7.9 in the model yields the second highest predicted mean SOC wt. % (1.2 wt %), consistent with the occurrence of deep calcareous buried soil in the Terrace sites. Previous work shows that exchangeable Ca binds to SOM and clay, leading to increased SOM stabilization and concentration (Rasmussen et al., 2018). This link between pH and landform was reconfirmed here using this recursive partitioning method and further shows that buried landscapes preserved in older landforms may have physicochemical properties different from the surface that promote SOC storage. This buried layer in the Terrace sites has a similar SOC content to that of the overlying surface soil and sediment (Fig. 6).

Lower mean SOC values are more common in Floodplains with X_{lf} of less than $2.37x10^{-7}$ kg/m^3. Although the label of buried vs. surface soil is not used in the pruned tree, landform retains information that improves prediction of SOC, where; samples are divided into either (i) Floodplain or (ii) Bar and Terrace sites with B or C horizons and pH <7.9. Buried or surface soils are still used to predict SOC, although indirectly. The selection of A horizons captured the majority of the surface soils, and the selection of pH ≥7.9 only occurs in buried layers.

4.3 Long-term differences in SOC turnover (β) by landform

The $\delta^{13}C_{soc}$ in all landforms and at all depth are consistent with the fractionation of carbon due to decomposition in the soil. The difference between mean surface and buried $\delta^{13}C_{soc}$, ranged from 1.5‰, 2‰, and 0.7‰ in the Bars, Floodplains, and Terraces, respectively. The differences in β (slope of the line of $\delta^{13}C_{soc}$ to log[SOC]) , as well as differences in mean layer $\delta^{13}C_{soc}$, suggest that Terraces have longer turnover rates than either Bars or Floodplains (Acton et al., 2013; Kramer and Gleixner, 2008; Garten Jr et al., 2000). That in combination with the local properties of the Terraces, such as the poor drainage and the more alkaline sediments at depth, due to the buried calcareous soil, promotes further stabilization rather than decomposition.

4.4 Comparison to Other Studies

The SOC stocks from our humid-subtropical study area are consistent with previous carbon-stock studies in valley bottoms but vary with the scale of the study and

with climate. A non-exhaustive literature review shows that four such studies focus on floodplains or overbank C stocks. Bullinger-Weber et al. (2014) calculate C stocks in restored floodplains of the Rhine, Emme, and Thur Rivers. Their study finds that floodplains in the Rhine have stocks of 1.21 ± 0.21 kg/m^2, the Emme have stocks of 1.88 ± 0.73 kg/m^2, and the Thur have stocks of 1.55 ± 0.32 kg/m^2. Two Rhine river studies by Hoffman et al., (2013, 2009) show that floodplains retain 5.0 ± 1.3 kg/m^2.

Clarks River floodplains retain the most SOC within the surface soils and have mean values in the range of the studies previously mentioned. However, the floodplains are spatially restricted (Fig. 2). The floodplains and bars comprised 24.7 % of the valley bottom area in our study area and while they experience deposition on a more regular basis, they only store a portion of the total SOC deposited within the valley bottom. Rather, the terrace landscape comprises 75.3 % of the Clarks River valley bottom study area and likely extend further upstream and downstream. The mean SOC stock of the Clarks River floodplains was 2.72 ± 0.20 kg/m^2, which is 54 % less than the Hoffman estimates (2013, 2009) and two times greater than the Bullinger-Weber estimates (2014). These differences to the Rhine studies may be due to elevation differences (alpine or non-alpine floodplains) and the differences in sampling depths further emphasizing the need to account for deeper C. The differences between Hoffman et al., (2013, 2009) and this study are likely due to differences in scale. This study only focused on a small portion of the Clarks River valley, and as such, the results are smaller than the larger Rhine valley meta-analysis (*ibid.*).

A study of floodplains along the Cosumnes River in northern California (D'elia et al., 2017) was also compared to the Clarks River. Cosumnes River SOC stock

calculations integrated to 1m in depth showed that floodplains contained 12.9 kg/m^2 (129 Mg/ha). When SOC stock were integrated to 3 m, which included a buried horizon, SOC stocks more than doubled to 28.6 kg/m^2 (286 Mg/ha). This increase with depth is consistent with our Clarks River findings and supports the argument that deeper soil horizons and buried horizons need to be accounted for when estimating SOC stocks. The 0 - 3 m stocks from the Cosumnes floodplains were less than all of the Floodplain sites (0 - 2.7 m) in the Clarks River (MZ_f = 76.8 ± 0.26 kg/m^2 TZ_f = 69.40 ± 0.40 kg/m^2 DC_f = 29.73 ± 0.14 kg/m^2). The results from the Cosumnes River differ from the Clarks River dataset likely due to climatic and vegetation differences as the Cosumnes River valley is located in a region with a Mediterranean climate. The differences in climate also likely reduce the amount of above ground biomass, with Clarks River being more densely forested than the Cosumnes River valley. This reduction in above ground biomass would limit the amount of C inputs to the soil.

CONCLUSION

Previous work shows that depositional sites have the potential to store SOC and that landform position does impact the fate of eroding SOC. In this study, data collected from the Clarks River valley in western Kentucky shows that buried SOC stocks were much greater than the stocks in the associated surface soils. These buried stocks made up over half of the SOC stocks in each landform. This study also demonstrates through a classification and regression tree analysis that valley bottom landscape position does play a role in SOC storage. The storage or oxidation of SOC at each landform appears to be driven by the varying physical and chemical properties of each landform position.

Within the Clarks River valley, Bars and Terraces retain more SOC through burial of woody debris and the inputs of local vegetation at the Bars and the stabilization and protection of older SOC at the Terraces. In contrast, the Floodplains oxidize SOC in more weakly developed and well drained soils. Deep calcareous layers in the Terraces that may have formed under different soil forming processes also had a legacy effect on the storage of SOC as exchangeable Ca was shown to bind to SOC more readily in alkaline soils and sediments. Notably, the pH variability of buried soils and landscape position play an important role in SOC storage, suggesting that future work focusing on valley-bottom depositional profiles should consider these effects on SOC storage.

TABLES

Table 1. Radiocarbon (RC) and modeled calendar ages from the Clarks River valley.

Landform	Site	Sample type	Sample depth (cm)	Lab code	pMC	1-σ error	RC (yr. BP = AD 1950)	1-σ error	Calendar age (PD) [1] (yr. BP= AD 2010)	Median age yr. BP[2]
Bar	MZ	wood debris	131-141	D-AMS 025714	116.83	0.39	modern (post-bomb)	-	51.59-50.97 (0.075) 24.14-24.13 (0.001) 22.89-22.71 (0.020) 22.12-19.82 (0.856) 19.58-19.12 (0.048)	21
Floodplain	MZ	charcoal	256-266	D-AMS 025715	92.91	0.26	591	22	707-644 627-601 (0.954)	666
Terrace	TZ	charcoal	60	D-AMS 025716	95.95	0.30	332	25	528-369 (0.954)	447
	MZ	$CaCO_3$	305	D-AMS 025717	41.05	0.15	7,152	29	8,076-7,998 (0.954)	8,036

[1](PD)= Relative area under probability distribution of calibration curve which is listed in parentheses following the age range. Modern (post-bomb) RC ages modeled using CALIBomb. Pre-Bomb ages calibrated using CALIB 7.1.

[2]The Median age in yr. BP is the median calibrated calendar age of the weighted PD.

Table 2. Soil organic carbon stocks for alluvial Bar sites along Clarks River. See Appendix 1, 4, & 7 for soil description details.

Site	Soil/Layer*	Horizon	Thickness (cm)	Horizon stock (kg/m^2)	Mean soil/layer stock (kg/m^2)	Mean site stock (kg/m^2)	Mean landform stock (kg/m^2)
MZ_b	Surface	A	3	0.57	1.48 ± 0.43	2.78 ± 0.48	2.16 ± 0.34
		AB	17	2.80			
		Bg1	10	1.29			
		Bg2	10	1.17			
		Bg3	15	1.58			
	Buried	2Ab1	3	0.29	3.49 ± 0.65		
		2Bg1b1	27	2.43			
		2Bg2b2	45	5.03			
		2Cg	26	3.10			
TZ_b	Surface	C1	12	0.45	0.68 ± 0.25	0.68 ± 0.25	
		C2	13	1.36			
		C3	7	0.47			
DC_b	Surface	Ag	10	0.82	1.90 ± 0.70	1.60 ± 0.43	
		Cg	34	2.44			
	Buried	2Cg2	14	1.16	1.16 ± 0.47		

*Soil/Layer refers to either surface soils, buried soils or lithologic discontinuities (LD). Both buried soils and LDs are referred as “buried layers”.

Table 3. Soil organic carbon stocks for alluvial Floodplain sites along Clarks River. See Appendix 2, 5, & 8 for soil description details.

Site	Soil/Layer	Horizon	Thickness (cm)	Horizon stock (kg/m^2)	Mean soil/layer stock (kg/m^2)	Mean site stock (kg/m^2)	Mean landform stock (kg/m^2)
MZ_f	Surface	A	7	0.88	3.22 ± 0.79	3.36 ± 0.26	2.72 ± 0.20
		Bwg	43	3.81			
	Buried	Bwg1b1	55	4.56	3.40 ± 0.29		
		Bwg2b1	45	2.43			
		Bwg3b2	50	2.73			
		2Cg	86	2.87			
TZ_f	Surface	A	4	0.53	2.47 ± 0.65	3.65 ± 0.43	
		Bw1	45	2.96			
	Buried	Bw2b1	100	5.27	4.07 ± 0.53		
		2Bw3b2	40	2.25			
		2Bw4b2	30	1.40			
DC_f	Surface	A	10	1.20	2.05 ± 0.52	1.29 ± 0.15	
		Bt	30	2.33			
	Buried	Bt2	40	2.14	1.13 ± 0.15		
		Bw	50	1.46			
		Bw2	20	0.43			
		2Bw3b1	30	0.77			
		2Bgb1	40	0.99			
		3Bg2b2	30	0.73			
		4Bg3b3	32	0.81			

Table 4. Soil organic carbon stocks for alluvial Terrace sites along Clarks River. See Appendix 3, 6, & 9 for soil description details. See Table 5 for additional alluvial Terrace sites.

Site	Soil/Layer	Horizon	Thickness (cm)	Horizon stock (kg/m^2)	Mean soil/layer stock (kg/m^2)	Mean site stock (kg/m^2)	Mean landform stock (kg/m^2)
MZ_t	Surface	O, A, AB	5	0.78	3.35 ± 0.65	3.78 ± 0.32	3.63 ± 0.20
		Btg1	25	2.56			
		Btg2	38	4.02			
	Buried	Btg3	43	5.48	3.88 ± 0.38		
		2Btg	34	2.49			
		2Btgss	32	2.18			
		2BC	23	1.33			
		2Btkgb1	65	4.03			
		2Btgb	20	1.20			
		2Btkgb2	45	5.52			
		2BCkgb	40	6.21			
		3Cg	9	0.92			
TZ_t	Surface	A	2	0.33	1.74 ± 0.29	4.01 ± 0.37	
		EBg	19	1.75			
		Btg1	28	1.88			
		Btg2	30	2.21			
	Buried	Btg3b	40	2.70	4.56 ± 0.41		
		2Btgssb	45	2.95			
		2Btg2b	45	2.85			
		2Btg3	70	3.80			
		2Btgkb	45	4.92			
		2Ctk1	50	8.28			
		2Ctk2	40	7.48			
		3Btgk1	20	3.51			

Table 5. Soil organic carbon stocks for alluvial Terrace sites along Clarks River. See Appendix 3, 6, & 9 for soil description details.

Site	Soil/Layer	Horizon	Thickness (cm)	Horizon stock (kg/m^2)	Mean soil/layer stock (kg/m^2)	Mean site stock (kg/m^2)	Mean landform stock (kg/m^2)
DC_t	Surface	A	3	0.52	1.93 ± 0.31	2.56 ± 0.34	3.63 ± 0.20
		Btg1	27	2.06			
		Btg2	24	1.88			
		Btg3	30	2.35			
	Buried	Btg4	16	1.40	3.28 ± 0.64		
		Btgb1	45	4.03			
CR_t	Surface	A	3	0.68	2.36 ± 0.65	3.10 ± 0.62	
		Btg1	21	2.44			
		Btg2	19	2.13			
		Btg3	34	4.12			
	Buried	2Bssgb	55	5.43	4.02 ± 1.22		
		2Btgb	27	2.07			
		2BCgb	29	3.16			

FIGURES

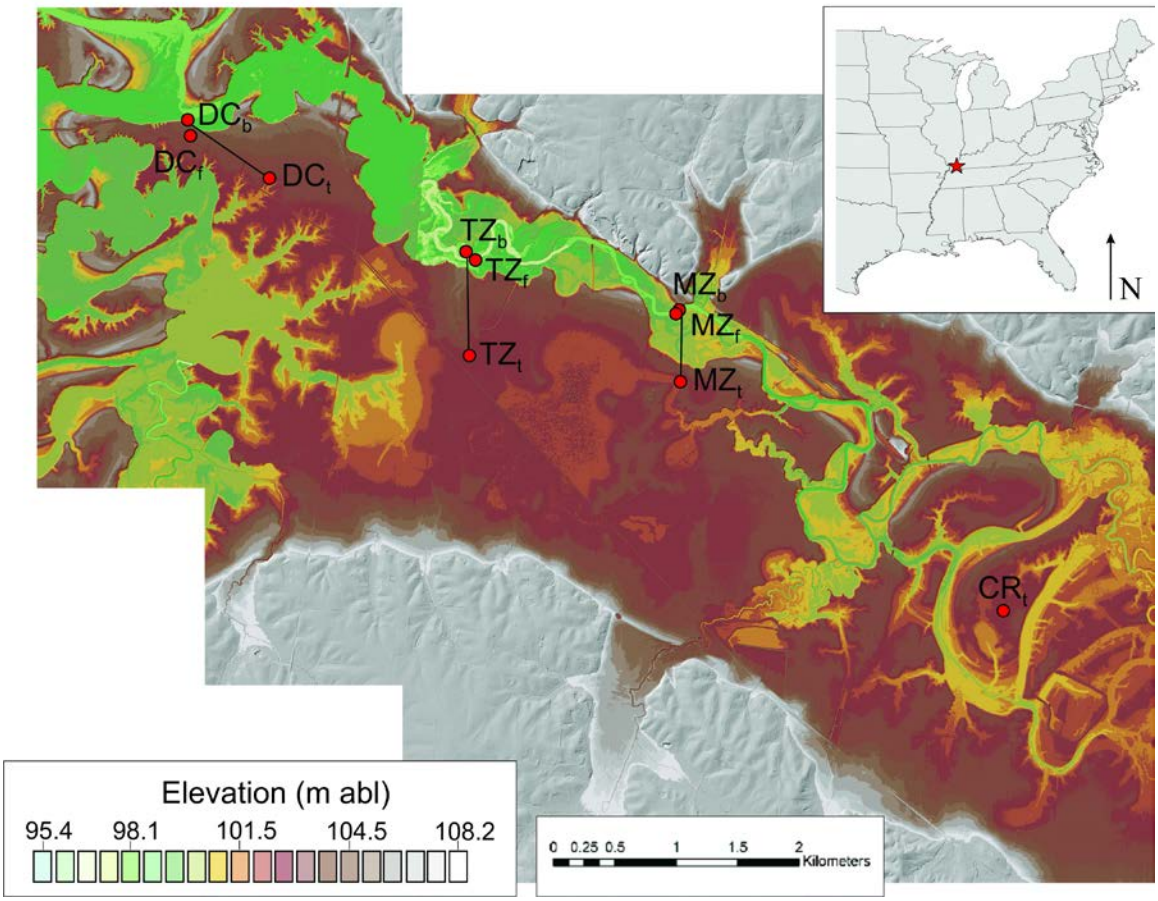

Figure 1. Clarks River study area. Inset map: mid-continent and eastern U.S.A. map showing location of study (red star). Main map: Elevation map and hill shade of the Clarks River study area. Color gradient shows results of digital elevation model, delineating surfaces between 95.4 and 108.2 m asl. Gray hill shade approximates upland and side slope landforms that drain into the Clarks River study area. Elevations corresponding to darker brown colors approximate the location of Terraces. Elevations corresponding to the green and tan colors denote the location of Floodplains and Bars. Cross-valley transects and landform sites are noted as black lines and red dots, respectively. Transect elevation profiles and sites are shown in figure 2.

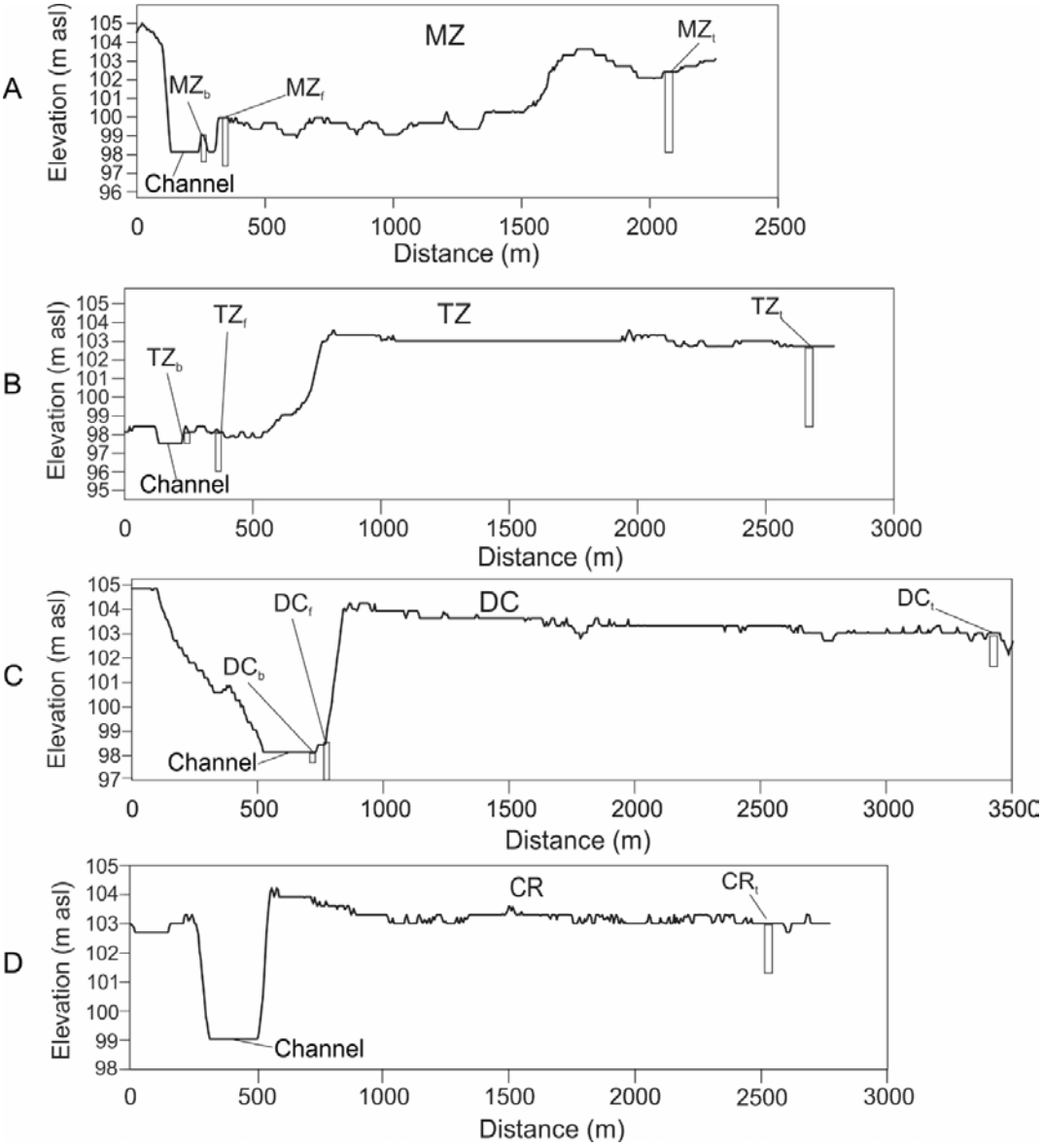

Figure. 2. Cross-valley elevation transects (downstream from A to C) showing the soil profile locations and depth of sampling landform sites sampled. (A) MZ transect showing location and depths of profiles sampled at each landform: Bar (MZ_b), Floodplain (MZ_f) and Terrace (MZ_t). (B) TZ transect showing location and depths of profiles sampled at each landform: Bar (TZ_b), Floodplain (TZ_f) and Terrace (TZ_t). (C) DC transect showing location and depths of profiles sampled at each landform: Bar (DC_b), Floodplain (DC_f) and Terrace (DC_t). (D) CR transect (upstream of A) showing location of Terrace site and depth of profile sampled (CR_t). See figure 1 for the transect and site location along the Clarks river valley.

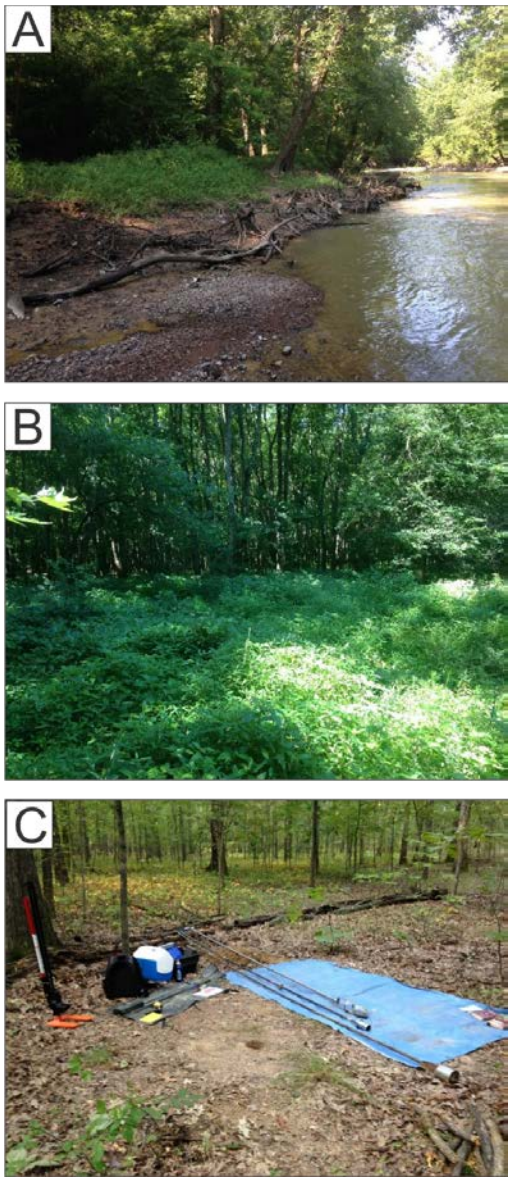

Figure 3. Examples of site setting for the three alluvial landscape positions studied along Clarks River. (A) Bar site (MZ_b), where samples were taken along the top of the vegetated Bar. Note the large woody debris deposited along the base of the Bar in the un-vegetated and more frequently inundated zone. (B) Floodplain site (MZ_f), where samples were taken in the open-canopy area with a dense understory. Dense herbaceous understory was common along Floodplains. (C) Terrace site (TZ_t) showing location of auger and bulk density coring hole to left of blue tarp. Note the low amount of herbaceous understory, a common feature along Clarks River Terraces dominated by *Quercus stellata* (post oak).

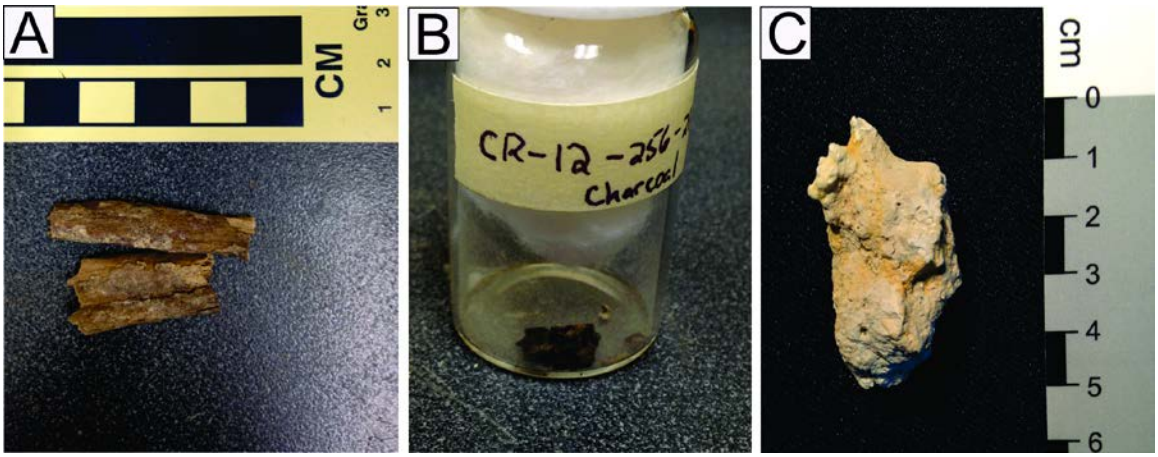

Figure 4. Radiocarbon samples. (A) Woody debris from MZ_b (B) Charcoal sample from MZ_f (C) Carbonate rhizolith collected from TZ_t. See Table 1 for associated ages.

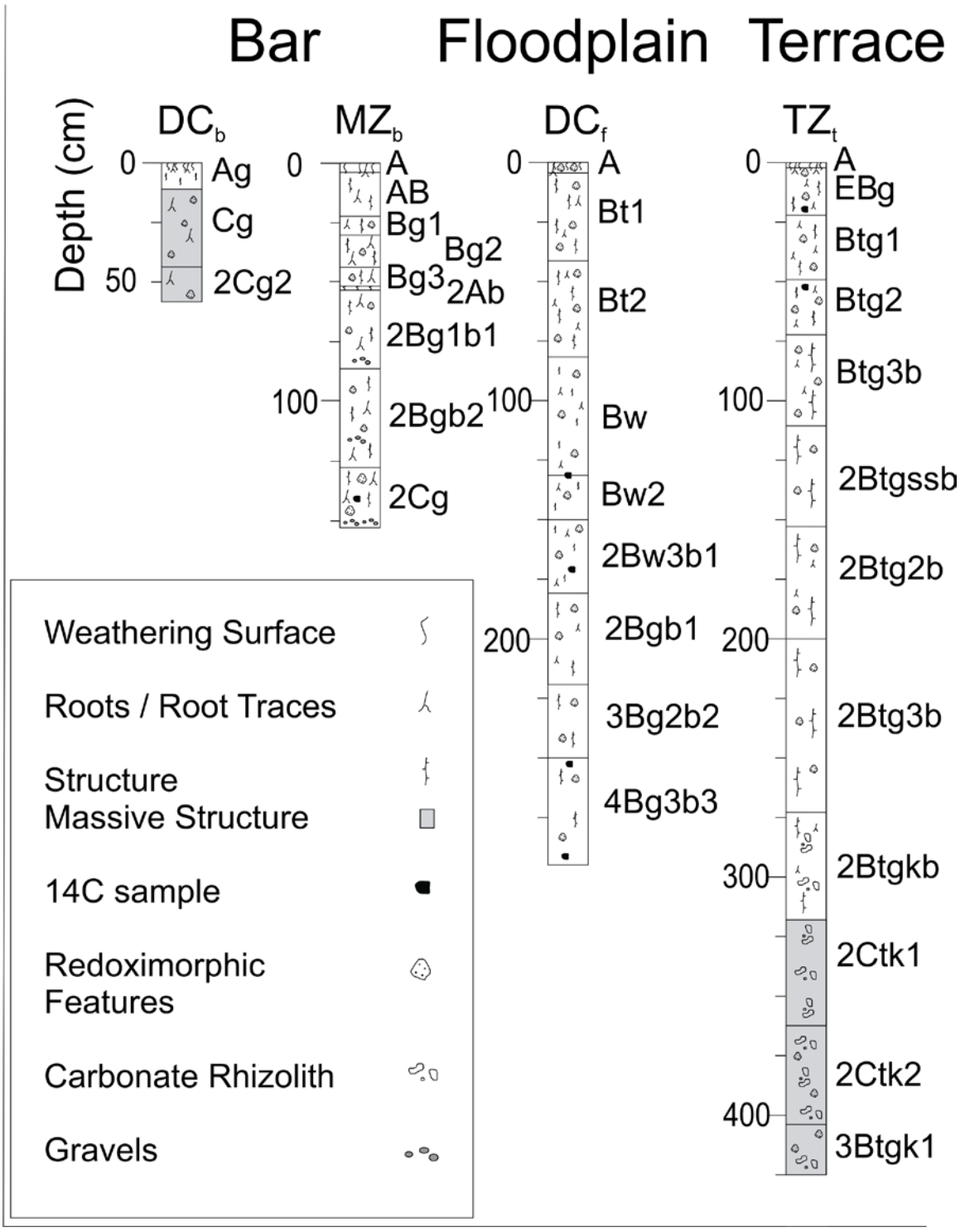

Figure 5. Soil profile examples for each landform type. Bars had two types of soil profiles, ranging from little soil development (DC_b) to fairly developed (MZ_b) and reached also varied in depth to refusal. Floodplains were weakly developed B and buried B horizons that ranged from 2.2 to 2.8 m in depth. Terraces reached 4 m in depth and contained multiple LDs as well as carbonate rhizoliths at 3 m in depth. See key for symbology.

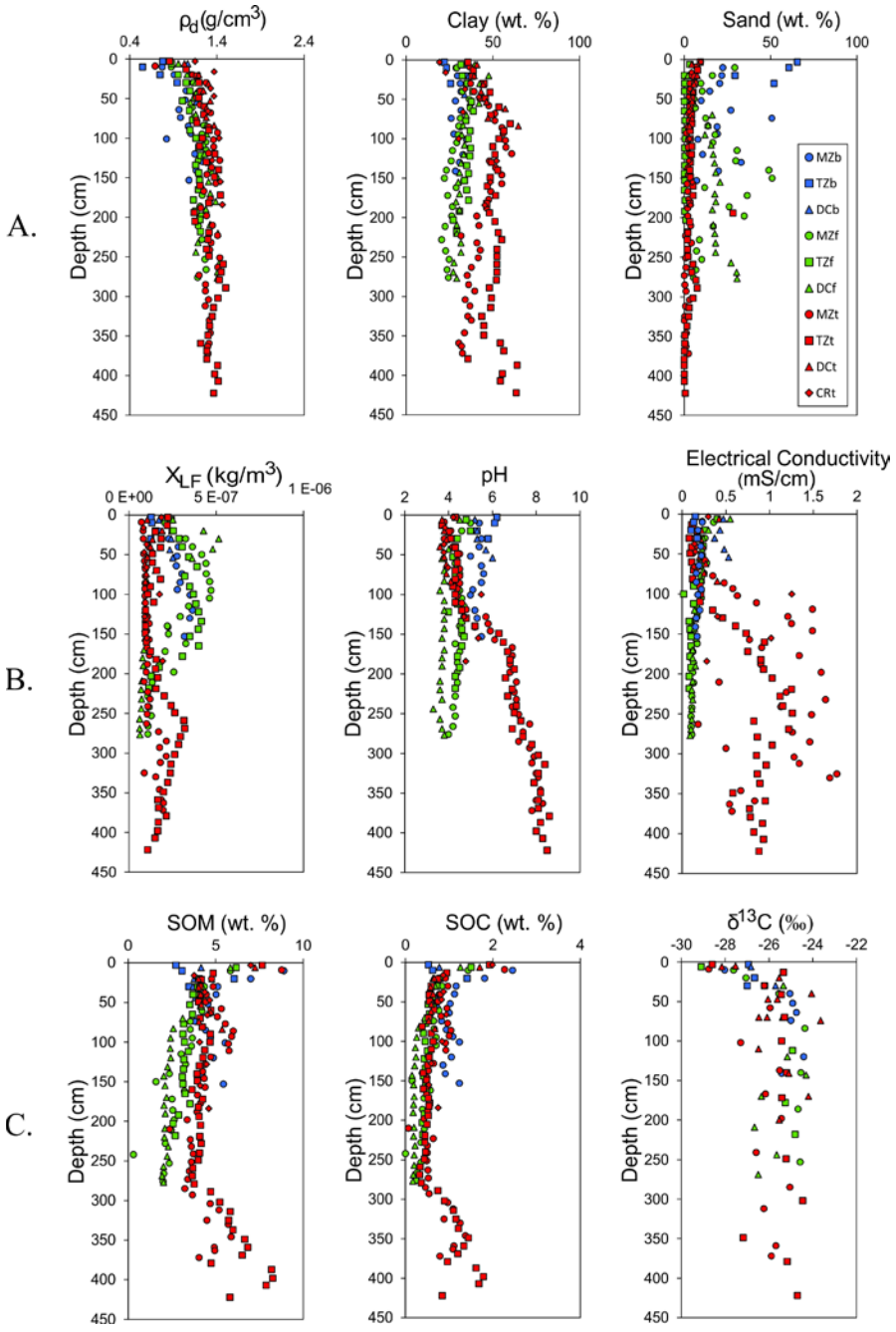

Figure 6. Physical, chemical and biological characteristics of the Clarks River soil and sediment profiles. See wt. % sand plot for symbology and color key. Landscape position corresponds to color: Bars are blue, Floodplains are green and Terraces are red. Refer to Fig. 3 for profile locations and Appendix 1 for profile descriptions.

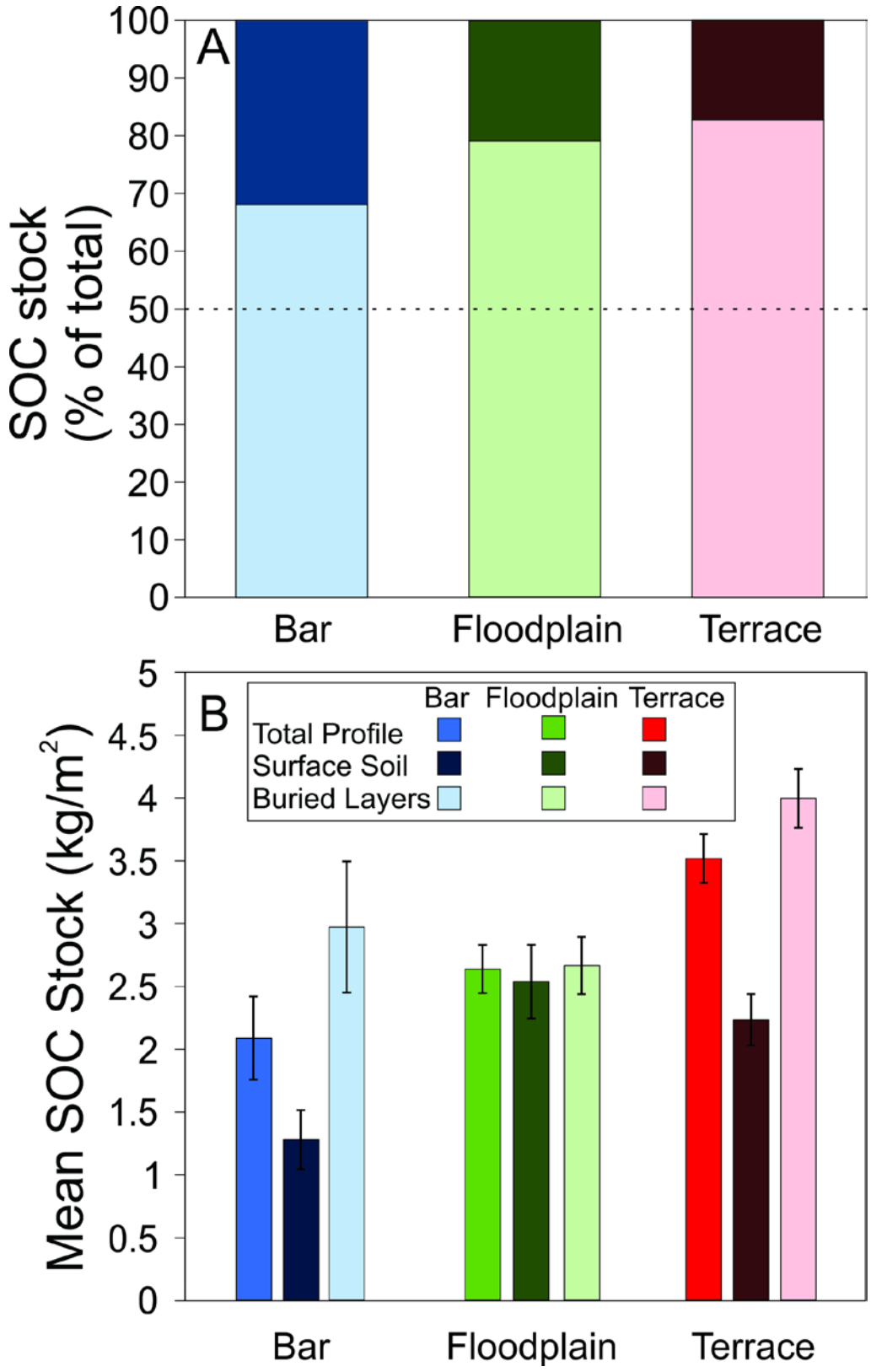

Figure 7. SOC stock calculations by landform position and layer position. (A) Total SOC stocks by landform. (B) Mean SOC stocks by landform. See color-shade key in B.

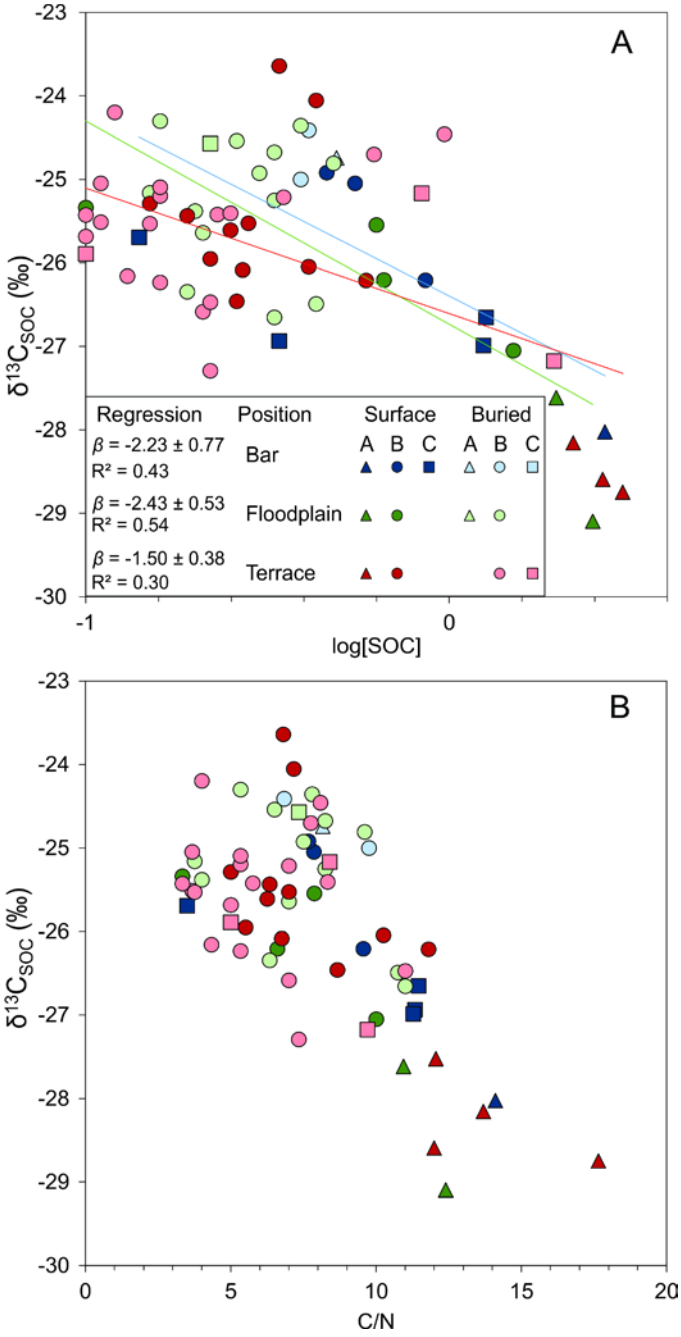

Figure 8. Isotope geochemistry of SOC by landform and soil horizon. (A) $\delta^{13}C_{SOC}$ against log[SOC] by landform position with regression lines and slope (β). Landform positions are color-coded and soil horizons are arranged by symbology. (B) $\delta^{13}C_{SOC}$ against C/N by landform position. See key in (A) for definitions of symbology in (B). Empty rows in key indicate the lack of those horizons in the profiles.

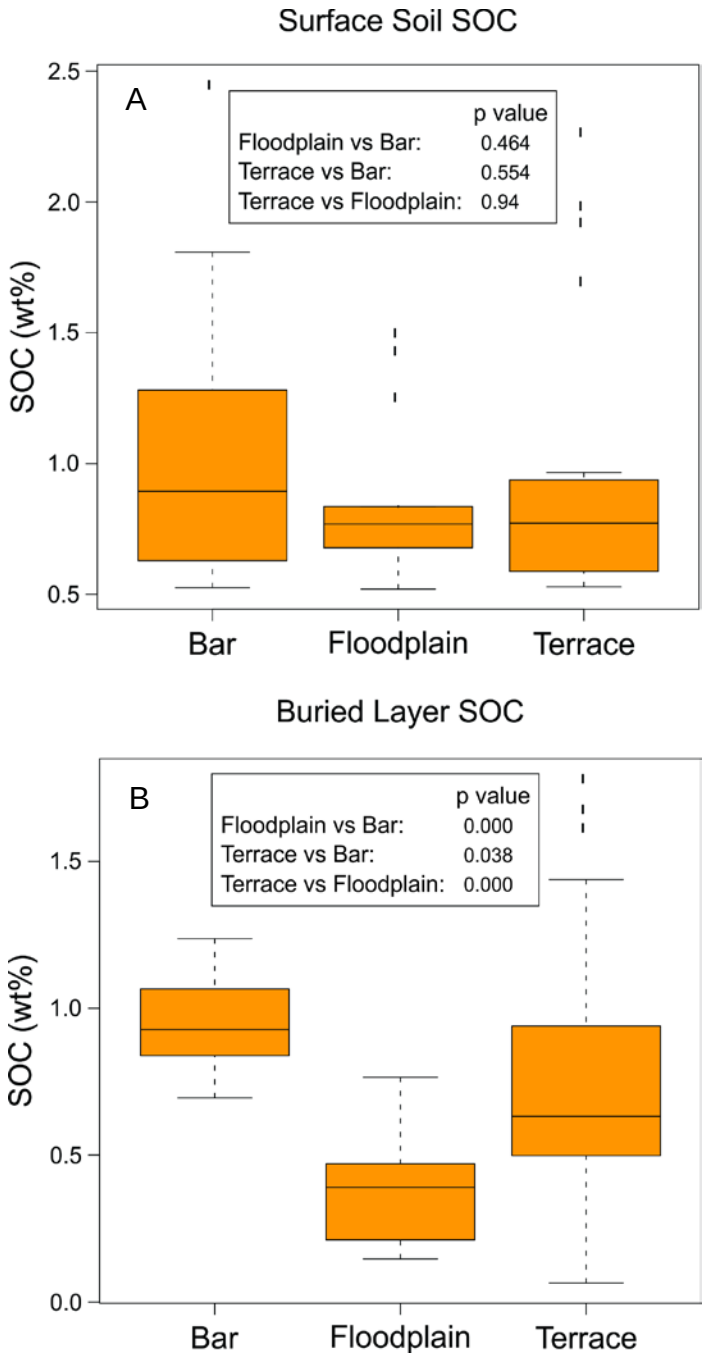

Figure 9. Box plots showing mean SOC in wt % for surface and buried layers. P values from Tukey HSD tests show variance in mean SOC wt % across landforms. P values show no statistical difference in surface SOC wt % by landform while buried layers in the Floodplains are statistically different from buried layers in both the Bar and Terrace.

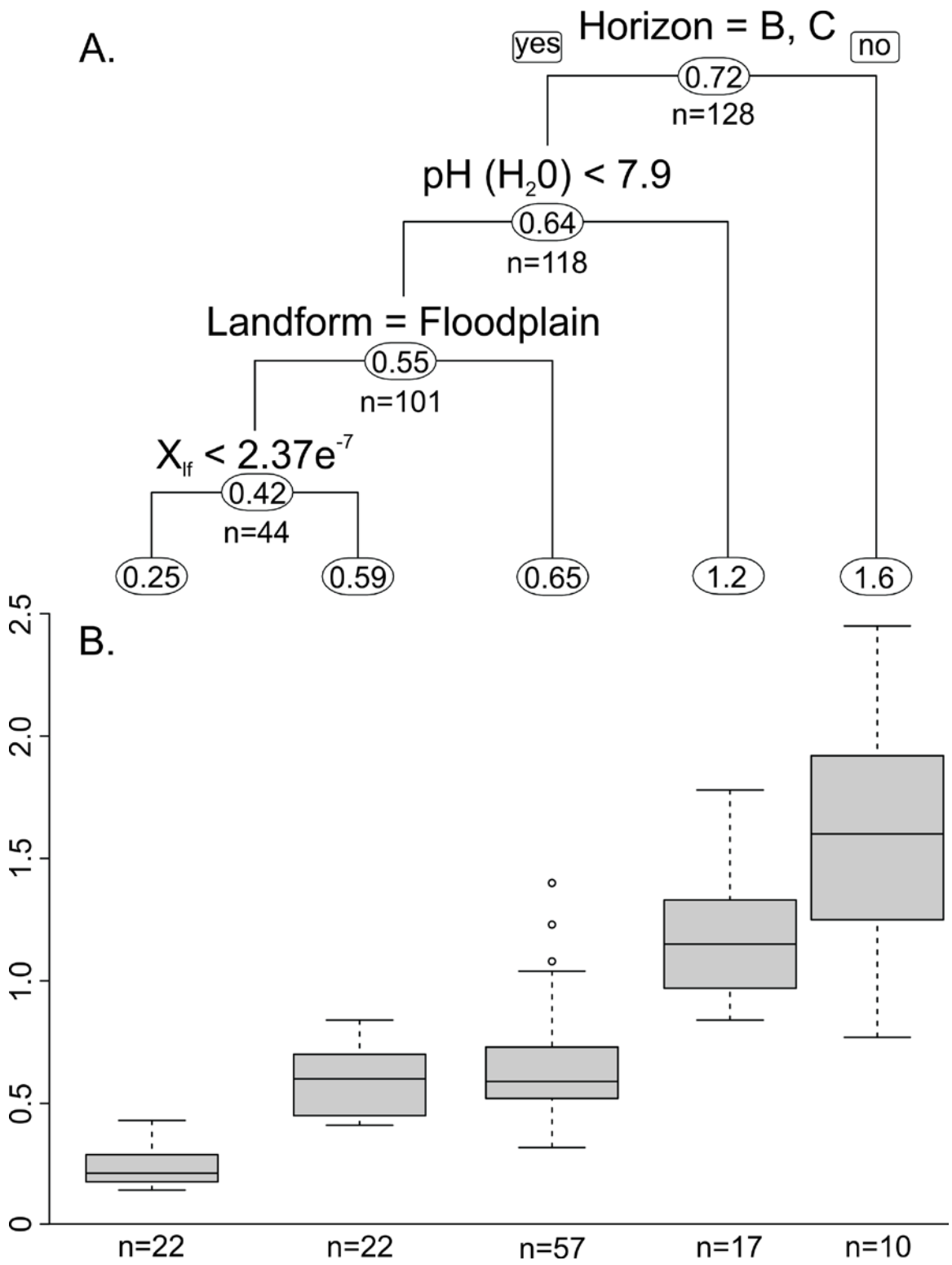

Figure 10. Pruned Classification and regression tree analysis output with mean SOC wt % for each terminal node. Terminal node box plots show the mean and distribution of SOC wt % at each branch in the regression tree. The model had a prediction error of ± 0.2 wt %

REFERENCES

Acton, P., Fox, J., Campbell, E., Rowe, H., Wilkinson, M., 2013. Carbon isotopes for estimating soil decomposition and physical mixing in well-drained forest soils. Journal of Geophysical Research: Biogeosciences 118, 1532–1545.

Ahr, S.W., Nordt, L.C., Schaetzl, R.J., 2016. Lithologic discontinuities in soils. International Encyclopedia of Geography: People, the Earth, Environment and Technology: People, the Earth, Environment and Technology 1–8.

Andrews, D.M., Lin, H., Zhu, Q., Jin, L., Brantley, S.L., 2011. Hot spots and hot moments of dissolved organic carbon export and soil organic carbon storage in the Shale Hills catchment. Vadose Zone Journal 10, 943–954.

Berhe, A.A., Harden, J.W., Harte, J., Torn, M.S., 2005. Soil degradation and global change: role of soil erosion and deposition in carbon sequestration.

Berhe, A.A., Harden, J.W., Torn, M.S., Harte, J., 2008. Linking soil organic matter dynamics and erosion-induced terrestrial carbon sequestration at different landform positions. Journal of Geophysical Research: Biogeosciences 113.

Berhe, A.A., Harte, J., Harden, J.W., Torn, M.S., 2007. The significance of the erosion-induced terrestrial carbon sink. AIBS Bulletin 57, 337–346.

Blazejewski, G.A., Stolt, M.H., Gold, A.J., Gurwick, N., Groffman, P.M., 2009. Spatial distribution of carbon in the subsurface of riparian zones. Soil Science Society of America Journal 73, 1733–1740.

Bullinger-Weber, G., Le Bayon, R.-C., Thébault, A., Schlaepfer, R., Guenat, C., 2014. Carbon storage and soil organic matter stabilisation in near-natural, restored and embanked Swiss floodplains. Geoderma 228, 122–131.

Cerling, T.E., 1984. The stable isotopic composition of modern soil carbonate and its relationship to climate. Earth and Planetary science letters 71, 229–240.

Chaopricha, N.T., Marín-Spiotta, E., 2014. Soil burial contributes to deep soil organic carbon storage. Soil Biology and Biochemistry 69, 251–264.

Cox, R.T., Larsen, D., Forman, S.L., Woods, J., Morat, J., Galluzzi, J., 2004. Preliminary assessment of sand blows in the southern Mississippi Embayment. Bulletin of the Seismological Society of America 94, 1125–1142.

Dearing, J.A., 1994. Environmental magnetic susceptibility: using the Bartington MS2 system. Chi Pub., Kenilworth

D'elia, A.H., Liles, G.C., Viers, J.H., Smart, D.R., 2017. Deep carbon storage potential of buried floodplain soils. Scientific reports 7, 8181.

Diefendorf, A.F., Mueller, K.E., Wing, S.L., Koch, P.L., Freeman, K.H., 2010. Global patterns in leaf 13C discrimination and implications for studies of past and future climate. Proceedings of the National Academy of Sciences 107, 5738–5743.

Doetterl, S., Berhe, A.A., Nadeu, E., Wang, Z., Sommer, M., Fiener, P., 2016. Erosion, deposition and soil carbon: a review of process-level controls, experimental tools and models to address C cycling in dynamic landscapes. Earth-Science Reviews 154, 102–122.

Driese, S.G., Li, Z.-H., McKay, L.D., 2008. Evidence for multiple, episodic, mid-Holocene Hypsithermal recorded in two soil profiles along an alluvial floodplain catena, southeastern Tennessee, USA. Quaternary Research 69, 276–291.

Fine, P., Verosub, K.L., Singer, M.J., 1995. Pedogenic and lithogenic contributions to the magnetic susceptibility record of the Chinese loess/palaeosol sequence. Geophysical Journal International 122, 97–107.

Garten Jr, C.T., Cooper, L.W., Post III, W.M., Hanson, P.J., 2000. Climate controls on forest soil C isotope ratios in the southern Appalachian Mountains. Ecology 81, 1108–1119.

Grimley, D.A., Arruda, N.K., Bramstedt, M.W., 2004. Using magnetic susceptibility to facilitate more rapid, reproducible and precise delineation of hydric soils in the midwestern USA. Catena 58, 183–213.

Harden, J.W., Sharpe, J.M., Parton, W.J., Ojima, D.S., Fries, T.L., Huntington, T.G., Dabney, S.M., 1999. Dynamic replacement and loss of soil carbon on eroding cropland. Global Biogeochemical Cycles 13, 885–901.

Hemelryck, H.V., Fiener, P., Oost, K.V., Govers, G., Merckx, R., 2010. The effect of soil redistribution on soil organic carbon: an experimental study. Biogeosciences 7, 3971–3986.

Hoffmann, T., Glatzel, S., Dikau, R., 2009. A carbon storage perspective on alluvial sediment storage in the Rhine catchment. Geomorphology 108, 127–137.

Hoffmann, T., Schlummer, M., Notebaert, B., Verstraeten, G., Korup, O., 2013. Carbon burial in soil sediments from Holocene agricultural erosion, Central Europe. Global Biogeochemical Cycles 27, 828–835.

Hoogsteen, M.J.J., Lantinga, E.A., Bakker, E.J., Groot, J.C.J., Tittonell, P.A., 2015. Estimating soil organic carbon through loss on ignition: effects of ignition conditions and structural water loss. European Journal of Soil Science 66, 320–328.

Jobbágy, E.G., Jackson, R.B., 2000. The vertical distribution of soil organic carbon and its relation to climate and vegetation. Ecological applications 10, 423–436.

Kirkels, F., Cammeraat, L.H., Kuhn, N.J., 2014. The fate of soil organic carbon upon erosion, transport and deposition in agricultural landscapes—a review of different concepts. Geomorphology 226, 94–105.

Kohn, M.J., 2010. Carbon isotope compositions of terrestrial C3 plants as indicators of (paleo) ecology and (paleo) climate. Proceedings of the National Academy of Sciences 107, 19691–19695.

Kramer, C., Gleixner, G., 2008. Soil organic matter in soil depth profiles: distinct carbon preferences of microbial groups during carbon transformation. Soil Biology and Biochemistry 40, 425–433.

Lawrence, C.R., Harden, J.W., Xu, X., Schulz, M.S., Trumbore, S.E., 2015. Long-term controls on soil organic carbon with depth and time: A case study from the Cowlitz River Chronosequence, WA USA. Geoderma 247, 73–87.

Leifeld, J., Kögel-Knabner, I., 2005. Soil organic matter fractions as early indicators for carbon stock changes under different land-use? Geoderma 124, 143–155.

Liu, S., Bliss, N., Sundquist, E., Huntington, T.G., 2003. Modeling carbon dynamics in vegetation and soil under the impact of soil erosion and deposition. Global Biogeochemical Cycles 17.

Luo, Z., Feng, W., Luo, Y., Baldock, J., Wang, E., 2017. Soil organic carbon dynamics jointly controlled by climate, carbon inputs, soil properties and soil carbon fractions. Global change biology 23, 4430–4439.

Maxbauer, D.P., Feinberg, J.M., Fox, D.L., Nater, E.A., 2017. Response of pedogenic magnetite to changing vegetation in soils developed under uniform climate, topography, and parent material. Scientific reports 7, 17575.

McCarty, G.W., Ritchie, J.C., 2002. Impact of soil movement on carbon sequestration in agricultural ecosystems. Environmental Pollution 116, 423–430.

Miller, R.O., Kissel, D.E., 2010. Comparison of soil pH methods on soils of North America. Soil Science Society of America Journal 74, 310–316.

Nadeu, E., Berhe, A.A., Vente, J. de, Boix-Fayos, C., 2012. Erosion, deposition and replacement of soil organic carbon in Mediterranean catchments: a geomorphological, isotopic and land use change approach. Biogeosciences 9, 1099–1111.

Nanson, G.C., 1986. Episodes of vertical accretion and catastrophic stripping: a model of disequilibrium flood-plain development. Geological Society of America Bulletin 97, 1467–1475.

Olive, W.W., 1966. Lake Paducah, of late Pleistocene age, in western Kentucky and southern Illinois. US Geological Survey Professional Paper 550, D87–D88.

Polyakov, V., Lal, R., 2004a. Modeling soil organic matter dynamics as affected by soil water erosion. Environment International 30, 547–556.

Polyakov, V., Lal, R., 2004b. Soil erosion and carbon dynamics under simulated rainfall. Soil Science 169, 590–599.

Post, W.M., Izaurralde, R.C., Jastrow, J.D., McCARL, B.A., Amonette, J.E., Bailey, V.L., Jardine, P.M., West, T.O., Zhou, J., 2004. Enhancement of carbon sequestration in US soils. AIBS Bulletin 54, 895–908.

Prasad, A.M., Iverson, L.R., Liaw, A., 2006. Newer classification and regression tree techniques: bagging and random forests for ecological prediction. Ecosystems 9, 181–199.

Quade, J., Cerling, T.E., Bowman, J.R., 1989. Systematic variations in the carbon and oxygen isotopic composition of pedogenic carbonate along elevation transects in the southern Great Basin, United States. Geological Society of America Bulletin 101, 464–475.

R Core Team, 2017. R: A Language and Environment for Statistical Computing [WWW Document]. The R-Project for Statistical Computing. URL https://www.r-project.org/ (accessed 10.8.18).

Rasmussen, C., Heckman, K., Wieder, W.R., Keiluweit, M., Lawrence, C.R., Berhe, A.A., Blankinship, J.C., Crow, S.E., Druhan, J.L., Pries, C.E.H., 2018. Beyond clay: towards an improved set of variables for predicting soil organic matter content. Biogeochemistry 137, 297–306.

Rasmussen, C., Torn, M.S., Southard, R.J., 2005. Mineral assemblage and aggregates control carbon dynamics in a California conifer forest. Soil Science Society of America Journal 69, 1711–1721.

Reimer, P.J., Bard, E., Bayliss, A., Beck, J.W., Blackwell, P.G., Ramsey, C.B., Buck, C.E., Cheng, H., Edwards, R.L., Friedrich, M., 2013. IntCal13 and Marine13 radiocarbon age calibration curves 0–50,000 years cal BP. Radiocarbon 55, 1869–1887.

Ritter, D.F., Kochel, R.C., Miller, J.R., 2002. Process geomorphology.

Rumpel, C., Kögel-Knabner, I., 2011. Deep soil organic matter—a key but poorly understood component of terrestrial C cycle. Plant and soil 338, 143–158.

Schimel, D.S., Braswell, B.H., Holland, E.A., McKeown, R., Ojima, D.S., Painter, T.H., Parton, W.J., Townsend, A.R., 1994. Climatic, edaphic, and biotic controls over storage and turnover of carbon in soils. Global biogeochemical cycles 8, 279–293.

Schoeneberger, P.J., 2012. Field book for describing and sampling soils. Government Printing Office.

Scull, P., Franklin, J., Chadwick, O.A., 2005. The application of classification tree analysis to soil type prediction in a desert landscape. Ecological Modelling 181, 1–15. https://doi.org/10.1016/j.ecolmodel.2004.06.036

Smith, S.V., Renwick, W.H., Buddemeier, R.W., Crossland, C.J., 2001. Budgets of soil erosion and deposition for sediments and sedimentary organic carbon across the conterminous United States. Global Biogeochemical Cycles 15, 697–707.

Soil Survey Staff, 2014a. Keys to Soil Taxonomy | NRCS Soils [WWW Document]. URL https://www.nrcs.usda.gov/wps/portal/nrcs/detail/soils/home/?cid=NRCS142P2_053580 (accessed 9.20.18).

Soil Survey Staff, 2014b. Kellogg Soil Survey Laboratory Methods Manual [WWW Document]. URL https://www.nrcs.usda.gov/Internet/FSE_DOCUMENTS/stelprdb1253872.pdf (accessed 11.14.18).

Soil Survey Staff, Natural Resources Conservation Service, United States Department of Agriculture, 2013. Official Series Description - NATALBANY Series [WWW Document]. Official Soil Series Descriptions. URL https://soilseries.sc.egov.usda.gov/OSD_Docs/N/NATALBANY.html (accessed 9.19.18).

Soil Survey Staff, Natural Resources Conservation Service, United States Department of Agriculture, 2001. Official Series Description - CASCILLA Series [WWW Document]. Official Soil Series Descriptions. URL https://soilseries.sc.egov.usda.gov/OSD_Docs/C/CASCILLA.html (accessed 9.19.18).

Stallard, R.F., 1998. Terrestrial sedimentation and the carbon cycle: coupling weathering and erosion to carbon burial. Global Biogeochemical Cycles 12, 231–257.

Starr, G.C., Lal, R., Malone, R., Hothem, D., Owens, L., Kimble, J., 2000. Modeling soil carbon transported by water erosion processes. Land Degradation & Development 11, 83–91.

Stuiver, M., Reimer, P.J., 1993. Calib 7.1 [WWW Document]. CALIB REV7.1.0. URL http://calib.org/calib/calib.html (accessed 9.19.18).

Sutfin, N.A., Wohl, E.E., Dwire, K.A., 2016. Banking carbon: a review of organic carbon storage and physical factors influencing retention in floodplains and riparian ecosystems. Earth Surface Processes and Landforms 41, 38–60.

Therneau, T., Atkinson, B., port, B.R. (producer of the initial R., maintainer 1999-2017), 2018. rpart: Recursive Partitioning and Regression Trees.

Van Oost, K., Govers, G., Quine, T.A., Heckrath, G., Olesen, J.E., De Gryze, S., Merckx, R., 2005. Landscape-scale modeling of carbon cycling under the impact of soil redistribution: The role of tillage erosion. Global Biogeochemical Cycles 19.

Van Oost, K., Quine, T.A., Govers, G., De Gryze, S., Six, J., Harden, J.W., Ritchie, J.C., McCarty, G.W., Heckrath, G., Kosmas, C., 2007. The impact of agricultural soil erosion on the global carbon cycle. Science 318, 626–629.

Van Oost, K., Verstraeten, G., Doetterl, S., Notebaert, B., Wiaux, F., Broothaerts, N., Six, J., 2012. Legacy of human-induced C erosion and burial on soil–atmosphere C exchange. Proceedings of the National Academy of Sciences 109, 19492–19497.

VandenBygaart, A.J., Gregorich, E.G., Helgason, B.L., 2015. Cropland C erosion and burial: Is buried soil organic matter biodegradable? Geoderma 239, 240–249.

Vervoort, R.W., Radcliffe, D.E., West, L.T., 1999. Soil structure development and preferential solute flow. Water Resources Research 35, 913–928.

Wang, Z., Doetterl, S., Vanclooster, M., van Wesemael, B., Van Oost, K., 2015a. Constraining a coupled erosion and soil organic carbon model using hillslope-scale patterns of carbon stocks and pool composition. Journal of Geophysical Research: Biogeosciences 120, 452–465.

Wang, Z., Van Oost, K., Govers, G., 2015b. Predicting the long-term fate of buried organic carbon in colluvial soils. Global Biogeochemical Cycles 29, 65–79.

APPENDICES

Appendix 1: Mosquito Zone, Bar soil profile description.

Horizon	Depth (cm)	Description
A	0-3	Light yellowish brown (10YR 6/4) sandy loam with weakly subangular blocky structure; common coarse roots
AB	3-20	Yellowish brown (10YR 5/4) sandy loam with subangular blocky structure; common coarse roots; mica present
Bg1	20-30	Dark yellowish brown (10YR 4/4) loam with subangular blocky structure; Yellowish red (5YR 5/6) redox concentrations and gray (10YR 6/1) redox depletions; few fine roots; redox features follow roots.
Bg2	30-40	Dark yellowish brown (10YR 4/4) silty clay loam with subangular blocky structure; common coarse roots with clay coatings.
Bg3	40-55	Dark yellowish brown (10YR 4/4) loam with subangular blocky structure; very pale brown (10YR 7/3) redox depletions; manganese concentrations present; common coarse to fine roots.
2Ab1	55-58	Dark yellowish brown (10YR 4/4) silty clay loam with subangular blocky structure; common medium to fine roots with clay coatings.
2Bg1b1	58-85	Dark yellowish brown (10YR 4/4) sandy loam with weakly subangular blocky structure; very pale brown (10YR 7/4) redox depletions; increase in sand and rock gravel content.
2Bg2b2	85-130	Dark yellowish brown (10YR 4/4) silty clay loam with weakly subangular blocky structure; very pale brown (10YR 7/4) redox depletions; common coarse roots; increased gravel content and moisture.
2Cg	130-156	Brown (10YR 4/3) sandy clay loam with weakly subangular blocky structure; common coarse roots with woody debris; strong brown (7.5YR 5/8) redox concentrations and pale brown (10YR 6/3) redox depletions; manganese concentrations; refusal.

Appendix 2: Mosquito Zone, Floodplain soil profile description.

Horizon	Depth (cm)	Description
A	0-7	Brown (10YR 5/3); sandy loam with subangular blocky structure; common medium to fine roots
Bw	7-50	Dark yellowish brown (10YR 4/4) silt loam with subangular blocky structure; common coarse to medium roots with Mn coatings and redox concentrations around roots; charcoal fragments present at 30 cm
Bw1b1	50-105	Dark yellowish brown (10YR 3/4) silty clay loam with subangular blocky structure; common fine roots with Mn concentrations; mica present
Bw2b1	105-150	Dark yellowish brown (10YR 4/4) sandy clay loam with subangular blocky structure; few medium to fine roots; mica present.
Bw3b2	150-200	Dark brown (7.5YR 3/3) silty clay loam with subangular blocky structure; very few fine roots; clay infilling in root traces.
2Cg	200-286	Yellowish brown (10YR 5/4) silty clay loam with subangular blocky to massive structure; gray (10YR 6/1) redox depletions Mn concentrations present; few fine roots; charcoal present; refusal at water table.

Appendix 3: Mosquito Zone, Terrace soil profile description.

Horizon	Depth (cm)	Description
O	0-2	Dark brown (7.5YR 3/2); common coarse roots
A	2-3	Dark grayish brown (10YR 4/2) clay loam with granular structure; common fine roots
AB	3-5	Light brownish gray (10YR 6/2) silty clay loam with granular structure; common medium to fine roots; mica present
Btg1	5-30	Brown (10YR 5/3) silty clay loam with subangular blocky structure; Yellowish red (5YR 5/6) redox concentrations and gray (10YR 6/1) redox depletions; few fine roots; redox features follow roots.
Btg2	30-68	Brownish yellow (10YR 6/6) silty clay loam with subangular blocky structure; light gray (10YR 7/1) redox depletions; common very fine roots; mica present.
Btg3	68-111	Brownish yellow (10YR 6/8) silty clay loam with subangular blocky structure; strong brown (7.5YR 5/8) redox concentrations and light brownish gray (10YR 6/2) redox depletions; manganese concentrations present; mica present; few fine roots.
2Btg	111-145	Pale brown (10YR 6/3) silty clay loam with subangular blocky structure; strong brown (7.5 YR 4/6) and reddish yellow (7.5 YR 7/8) redox concentrations; very dark brown (10YR 2/2) redox depletions; manganese coatings; compact.
2Btgss	145-177	Dark gray (10YR 4/1) silty clay loam with subangular blocky structure; reddish yellow (7.5YR 6/8) redox concentrations and gray (10YR 6/1) redox depletions; Mn concentrations; few fine roots with Mn coatings around roots; slickensides; mica present
2BC	177-200	Light yellowish brown (10YR 6/4) silty clay loam with sub angular blocky structure; few medium to fine roots and pores; Charcoal fragments and mica present.
2Btkgb1	200-265	Yellowish brown (10YR 5/4) silty clay loam with subangular blocky structure; few fine to medium roots; manganese nodules and channel infills around root traces; clay coatings inside Mn tubules; carbonate nodules and coatings along roots.
2Btgb	265-285	Strong brown (7.5YR 5/8) silty clay loam with subangular blocky structure; manganese concentrations and clay coatings along root traces; Mn channel infills; fine mica present.
2Btkgb2	285-330	Grayish brown (10YR 5/2) silty clay loam with subangular blocky structure; strong brown (7.5YR 5/8) redox concentrations; Mn channel infills; few fine roots; clay coatings; diffuse lower boundary with loss of strong brown color.
2BCkgb	330-370	Grayish brown (10YR 5/2) silty clay loam with subangular blocky structure; strong brown (7.5YR 5/8) redox concentrations with gray (10YR 6/1) redox depletions; few fine roots; fine spherical Mn concentrations.
3Cg	370-379	Brownish yellow (10YR 6/6) silty clay loam with subangular blocky structure; light brownish gray (10YR 6/2) redox depletions; laminations and very fine pore spaces; refusal at water table

Appendix 4: Twilight Zone, Bar soil profile description.

Horizon	Depth (cm)	Description
C1	0-12	Strong brown (7.5YR 5/6) unconsolidated sand and gravels with no structure; young vegetation with few medium to fine roots.
C2	12-25	Dark yellowish brown (10YR 4/6) clay loam with massive structure; strong brown (7.5YR 5/6) redox concentrations and gray (10YR 5/1) redox depletions; buried woody debris; no roots.
C3	25-32	Strong brown (7.5YR 5/6) unconsolidated sand and gravels with no structure; no roots; refusal.

Appendix 5: Twilight Zone, Floodplain soil profile description.

Horizon	Depth (cm)	Description
Ag	0-4	Dark yellowish brown (10YR 4/4); silty clay loam with granular structure; common coarse to medium roots; strong brown (7.5YR 4/6) redox concentrations along roots; mica present.
Bwg1	4-50	Dark yellowish brown (10YR 4/4) silty clay loam with subangular blocky structure; common coarse to fine roots; light brownish gray (10YR 6/2) redox depletions and strong brown (7.5YR 4/6) redox concentrations; charcoal fragments present at 30 cm; very fine mica present.
Bwg2b1	50-150	Dark yellowish brown (10YR 4/6) silty clay loam with subangular blocky structure; common medium to fine roots; strong brown (7.5YR 5/8) redox concentrations and light yellowish brown (10YR 6/4) redox depletions; burrow at 50 cm; charcoal at 90 cm; diffuse boundary.
2Bwg3b2	150-190	Dark yellowish brown (10YR 4/4) silty clay loam with subangular blocky structure; common medium to fine roots with manganese and clay coatings; light brownish gray (10YR 5/8) redox depletions; charcoal at 160cm.
2Bwg4b2	190-220	Yellowish brown (10YR 5/4) silty clay loam with subangular blocky structure; strong brown (7.5YR 5/6) redox concentrations and light gray (2.5YR 7/1) redox depletions; manganese concentrations; very fine mica present.

Appendix 6: Twilight Zone, Terrace soil profile description.

Horizon	Depth (cm)	Description
A	0-2	Brown (10YR 5/3) loam with granular structure; common coarse to medium roots
EBg	2-21	Light gray (10YR 7/2) weakly mottled silt loam with weakly subangular blocky structure; common coarse to medium roots; yellow (10YR 7/6) redox concentrations; charcoal at 20cm; very dry.
Btg1	21-49	Light brownish brown (10YR 6/4) silty clay loam with subangular blocky structure; common coarse to medium roots; yellowish brown (10YR 5/8) redox concentrations and light gray (10YR 7/1) redox depletions; charcoal at 45-49 cm.
Btg2	50-70	Brownish yellow (10YR 6/8) silty clay loam with subangular blocky structure; Yellowish brown (10YR 5/8) redox concentrations and gray (10YR 5/1) redox depletions; common coarse roots with clay coatings; manganese concentrations; charcoal at 60cm; increase in clay content; diffuse boundary.
Btg3b	70-110	Grayish brown (10YR 5/2) silty clay loam with subangular blocky structure; strong brown (7.5YR 5/6) redox concentrations; few medium to fine roots with clay coatings; manganese concentrations; very fine mica present.
2Btgssb	110-155	Dark gray (10YR 4/1) silty clay loam with subangular blocky structure; strong brown (7.5YR 4/6) redox concentrations and light gray (10YR 7/2) redox depletions; manganese concentrations increase; slickensides; very dense.
2Btg2b	155-200	Yellow brown (10YR 5/6) silty clay loam with subangular blocky structure; gray (10YR 5/1) and light gray (10YR 7/1) redox depletions; manganese coatings; few medium to fine roots with clay coatings; mica present; clear gradual boundary.
2Btg3	200-270	Yellow brown (10YR 5/6) silty clay loam with subangular blocky structure; gray (10YR 5/1) redox depletions; Manganese concentrations; mica present; possible carbonate.
2Btgkb	270-315	Yellowish brown (10YR 5/4) silty clay loam with subangular blocky to massive structure; very few fine to very fine roots; carbonate rhizoliths; increase in manganese concentrations and clay coatings; mica present.
2Ctk1	315-365	Light yellowish brown (10YR 6/4) silty clay loam with massive structure; carbonate rhizoliths; loss of manganese concentrations and roots.
2Ctk2	365-405	Yellowish brown (7.5YR 5/8) silty clay loam with massive to platy structure; very pale brown (10YR 8/2) redox depletions; manganese concentrations return; clay coatings; carbonate rhizolith.
3Btgk1	405-425	Light brownish gray (10YR 6/2) silty clay loam with massive structure; strong brown (7.5YR 5/8) redox concentrations; manganese concentrations; carbonate rhizolith.

Appendix 7: Dry Coyote, Bar soil profile description.

Horizon	Depth (cm)	Description
Ag	0-10	Dark brown (10YR 3/3) silty clay loam with very fine granular structure; few fine roots; pale brown (10YR 6/3) redox depletions.
Cg	10-44	Dark brown (10YR 3/3) silty clay loam with massive structure; pale brown (10YR 6/3) redox depletions; few fine roots; mica present.
2Cg2	44-58	Dark yellowish brown (10YR 4/4) sandy clay loam with massive structure, yellowish brown (10YR 5/8) redox concentrations and light brownish gray (10YR 6/2) redox depletions; common medium to very fine roots; water table; refusal.

Appendix 8: Dry Coyote, Floodplain soil profile description.

Horizon	Depth (cm)	Description
A	0-10	Dark yellowish brown (10YR 3/4) silt loam with granular structure; common coarse to very fine roots with clay coatings; pale brown (10YR 6/3) redox depletions.
Bt	10-40	Dark yellowish brown (10YR 4/4) clay loam with angular blocky structure; common coarse to fine roots with clay coatings; pale brown (10YR 6/3) redox depletions; mica present.
Bt2	40-80	Dark yellowish brown (10YR 4/4) clay loam with angular blocky structure; common coarse to fine roots with clay coatings; mica present.
Bw	80-130	Yellowish brown (10YR 5/4) silty clay loam with weakly angular blocky structure; strong brown (7.5YR 5/8) redox concentrations and light brownish gray (10YR 6/2) redox depletions; few fine to very fine roots; mica present.
Bw2	130-150	Yellowish brown (10YR 5/4) sandy clay loam with weakly angular blocky structure; light brownish gray (10YR 6/2) redox depletions; few fine to very fine roots; very fine mica present; charcoal at 130cm.
2Bw3b1	150-180	Yellowish brown (10YR 5/4) sandy clay loam with weakly angular blocky structure; strong brown (7.5YR 5/8) redox concentrations and light brownish gray (10YR 6/2) redox depletions; few fine to very fine roots; charcoal at 170cm; clay coatings in root traces; mica present.
2Bgb1	180-220	Yellow brown (10YR 5/4) sandy clay loam with angular blocky structure; light brownish gray (10YR 6/2) redox depletions and strong brown (7.5YR 5/8) redox concentrations; few very fine roots; mica present.
3Bg2b2	220-250	Light yellow brown (10YR 6/4) silty clay loam with angular blocky structure; gray (7.5YR 6/1) redox depletions and reddish yellow (7.5YR 6/8) redox concentrations; mica present; loss of roots.
4Bg3b3	250-282	Light yellowish brown (10YR 6/4) silty clay loam with angular blocky structure; reddish yellow (7.5YR 6/8) redox concentrations and gray (7.5YR 6/1) redox depletions; no roots; mica present; charcoal at 280cm.

Appendix 9: Dry Coyote, Terrace soil profile description.

Horizon	Depth (cm)	Description
A	0-3	Brown (10YR 4/3) loam with granular structure; common coarse to fine roots; some decaying OM.
Btg1	3-30	Yellowish brown (10YR 5/4) silty clay loam with angular blocky structure; common coarse to fine roots with clay coatings; gray (10YR 6/1) redox depletions and yellowish brown (10YR 5/8) redox concentrations; mica present; manganese concentrations begin..
Btg2	30-54	Brownish yellow (10YR 6/6) silty clay loam with angular blocky structure; strong brown (7.5YR 5/8) redox concentrations and gray (10YR 6/1) redox depletions; manganese concentrations associated with redox features; common fine to very fine roots; very fine mica present; increase in density.
Btg3	54-84	Light yellowish brown (10YR 6/4) silty clay loam with angular blocky structure; strong brown (7.5YR 5/8) redox concentrations and gray (10YR 6/1) redox depletions; few medium to fine roots with clay coatings; charcoal at 55cm; manganese concentrations.
Btg4	84-100	Light yellowish brown (10YR 6/4) silty clay loam with angular blocky structure; gray (10YR 6/1) redox depletions and strong brown (7.5YR 5/8) redox concentrations; few medium to fine roots with clay coatings; manganese concentrations; consistency weakens; drier and moderately hard but crumbles.
Btgb1	100-145	Light brownish gray (10YR 6/2) grayish brown (10YR 5/2) redox depletions and strong brown (7.5YR 5/8) redox concentrations; silty clay loam with angular blocky structure; few fine to very fine roots; manganese concentrations and coatings along channel pores; very fine distinct discontinuous clay coatings, light brownish gray (10YR 6/2) in color along ped faces and channel pores; very fine mica.

Appendix 10: Alluvial Bar sites, elemental analyzer results.

Landform	Site	Layer	Horizon	Depth (cm)		SOC wt %	δ13C	δ15N	N wt %	C/N
Bar	MZ_b	Surface	A	0	10	2.68	-28.0	6.3	0.19	14.11
			Bg1	20	30	0.86	-26.2	7.8	0.09	9.56
			Bg2	30	40	0.55	-25.0	8.7	0.07	7.86
			Bg3	42	52	0.46	-24.9	8.7	0.06	7.67
		Buried	2Bg1b1	55	64	0.49	-24.7	8.4	0.06	8.17
			2Bg1b1	65	74	0.39	-24.9	8.8	0.04	9.75
			2Bg2b2	109	120	0.41	-24.4	8.9	0.06	6.83
			2Cg	131	141	0.42	-25.4	6.9	0.05	8.40
	TZ_b	Surface	C1	0	3	0.34	-26.9	7.3	0.03	11.33
			C2	10	20	1.26	-26.6	6.8	0.11	11.45
			C3	20	30	1.24	-26.9	6.4	0.11	11.27
	DC_b	Surface	Ag	0	6	1.03	-26.8	7.0	0.1	10.30
			Cg	20	30	0.14	-25.6	4.8	0.04	3.50
		Buried	2Cg2	44	54	1.05	-	4.9	0.04	26.25

Appendix 11: Alluvial Floodplain sites, elemental analyzer results.

Landform	Site	Layer	Horizon	Depth (cm)		SOC wt %	δ13C	δ15N	N wt %	C/N
Floodplain	MZ_f	Surface	A	0	10	1.97	-27.6	5.6	0.18	10.94
			Bwg	10	20	1.5	-27.0	6.3	0.15	10.00
			Bwg	30	40	0.63	-25.5	8.0	0.08	7.88
		Buried	Bwg1b1	74	84	0.39	-24.3	7.8	0.05	7.80
			Bwg2b1	130	140	0.26	-24.5	8.0	0.04	6.50
			Bwg3b2	175	186	0.33	-24.6	7.1	0.04	8.25
			2Cg	243	253	0.22	-24.5	7.6	0.03	7.33
	TZ_f	Surface	A	0	6	2.48	-29.1	6.3	0.2	12.40
			Bw1	20	30	0.66	-26.2	8.2	0.1	6.60
		Buried	Bw2b1	102	112	0.3	-24.9	6.9	0.04	7.50
			2bw3b2	168	178	0.33	-25.2	7.0	0.04	8.25
			2Bw4b2	208	218	0.48	-24.8	6.6	0.05	9.60
	DC_f	Surface	A	0	6	0.68	-	7.1	0.04	17.00
			Bt	20	30	0.1	-25.3	5.7	0.03	3.33
		Buried	Bt2	60	70	0.2	-25.3	5.1	0.05	4.00
			Bw	110	120	0.15	-25.1	5.4	0.04	3.75
			Be2	133	143	0.16	-24.3	5.0	0.03	5.33
			2Bw3b1	160	170	0.19	-26.3	5.1	0.03	6.33
			2Bgb1	200	209	0.33	-26.6	5.2	0.03	11.00
			3Bg2b2	238	244	0.21	-25.6	6.0	0.03	7.00
			4Bg3b3	260	269	0.43	-26.5	3.0	0.04	10.75

Appendix 12: Alluvial Terrace sites, elemental analyzer results.

Landform	Site	Layer	Horizon	Depth (cm)		SOC wt %	δ13C	δ15N	N wt %	C/N
Terrace	MZ_t	Surface	O, A, AB	0	9	3	-28.7	3.5	0.17	17.65
			Btg1	20	30	0.59	-26.2	6.4	0.05	11.80
			Btg2	49	58	0.22	-25.9	7.0	0.04	5.50
		Buried	Btg3	93	102	0.22	-27.3	6.0	0.03	7.33
			2Btg	128	137	0.11	-25.5	5.4	0.03	3.67
			2Btgss	158	167	0.13	-26.1	4.2	0.03	4.33
			2BC	188	198	0.1	-25.4	3.7	0.03	3.33
			2Btkgb1	232	241	0.21	-26.5	3.4	0.03	7.00
			2Btgb	275	285	0.11	-25.0	3.8	0.03	3.67
			2Btkgb2	307	312	0.16	-26.2	4.3	0.03	5.33
			2BCkgb	349	359	0.1	-25.7	6.2	0.02	5.00
			3Cg	368	372	0.1	-25.9	6.1	0.02	5.00
	TZ_t	Surface	A	0	3	2.64	-28.6	1.1	0.22	12.00
			EBg	3	13	0.28	-25.3	7.6	0.05	5.60
			Btg1	31	41	0.19	-25.4	8.0	0.03	6.33
			Btg2	60	70	0.15	-25.3	7.6	0.03	5.00
		Buried	Btg3b	90	100	0.23	-25.4	8.0	0.04	5.75
			2Btgssb	130	140	0.16	-25.2	7.7	0.03	5.33
			2Btg2b	163	172	0.25	-25.4	6.9	0.03	8.33
			2Btg3	241	249	0.35	-25.2	7.9	0.05	7.00
			2Btgkb	291	302	0.97	-24.4	7.4	0.12	8.08

		2Ctk1	340	349	1.94	-27.2	6.9	0.2	9.70
		2Ctk2	370	379	0.84	-25.1	8.2	0.1	8.40
		3Btgk1	412	422	0.62	-24.7	7.8	0.08	7.75
DC_t	Surface	A	0	6	2.19	-28.1	1.2	0.16	13.69
		Btg1	10	20	0.28	-25.5	7.2	0.04	7.00
		Btg2	31	40	0.43	-24.0	7.9	0.06	7.17
		Btg3	65	74	0.34	-23.6	7.8	0.05	6.80
CR_t	Surface	A	0	5	1.93	-27.5	2.5	0.16	12.06
		Btg1	15	47	0.41	-26.0	7.6	0.04	10.25
		Btg1	15	47	0.25	-25.6	8.4	0.04	6.25
		Btg2	47	70	0.27	-26.1	6.6	0.04	6.75
		Btg3	47	70	0.26	-26.4	8.7	0.03	8.67
	Buried	2Bssgb	70	110	0.22	-26.4	5.5	0.02	11.00
		2Bssgb	110	141	0.16	-25.1	5.6	0.03	5.33
		2Btgb	141	170	0.12	-24.2	6.9	0.03	4.00
		2BCgb	170	200	0.15	-25.5	6.3	0.04	3.75

Appendix 13: Soil organic carbon linear regression results comparing SOC correction factor to SOC measured by elemental analyzer.

Regression Statistics	
Multiple R	0.886591362
R Square	0.786044243
Adjusted R Square	0.783369796
Standard Error	0.420421423
Observations	82

ANOVA

	df	*SS*	*MS*	*F*	*Significance F*
Regression	1	51.94965638	51.94965638	293.9090795	1.63246E-28
Residual	80	14.14033386	0.176754173		
Total	81	66.08999024			

	Coefficients	*Standard Error*	*t Stat*	*P-value*	*Lower 95%*	*Upper 95%*	*Lower 95.0%*	*Upper 95.0%*
Intercept	-0.20986156	0.071580054	-2.931844128	0.004392203	-0.352310407	-0.067412714	-0.352310407	-0.067412714
X Variable 1	1.00989913	0.058907623	17.1437767	1.63246E-28	0.892669225	1.127129035	0.892669225	1.127129035

The correction factor is compared to the SOC measured by the elemental analyzer using a linear regression model. The model is shown to have an R^2 value of 0.78.